T.R.
BOLU ABANT İZZET BAYSAL UNIVERSITY
INSTITUTE OF GRADUATE STUDIES
Department of Physics

INFLUENCE OF INDUCTION HEATING ON THE PHYSICAL PROPERTIES OF IRON SHEATHED MgB_2

MASTER OF SCIENCE

AHMED RAJAB AHMED

ACADEMIC SUPERVISOR
Prof. Dr. Mustafa AKDOĞAN

BOLU, JULY - 2023

APPROVAL OF THE THESIS

INFLUENCE OF INDUCTIOUN HEATING ON THE PHYSICAL PROPERTIES OF IRON SHEATHED MgB_2 submitted by **Ahmed Rajab AHMED** and defended before the Examining Committe Members listed below in partial fulfillment of the requirements for the degree of **Master of Science** in **Department of Physics, Institute of Graduate Studies of Bolu Abant Izzet Baysal University in 25.07.2023** by

Examining Committee Members	**Signature**
Supervisor Prof. Dr. Mustafa AKDOĞAN Bolu Abant İzzet Baysal University	....
Member Prof. Dr. Serap SAFRAN Ankara University	....
Member Assoc. Prof. Dr. Murat OLUTAŞ Bolu Abant İzzet Baysal University	....

Prof. Dr. İbrahim KÜRTÜL
Director of Institute of Graduate Studies

ETHICAL DECLARATION

In this thesis dissertation that was properly prepared according to the Thesis Writing Rules of Bolu Abant İzzet Baysal University of the Institute of Graduates Studies, I hereby declare that;

- All data, information, and documents presented in the thesis were obtained in accordance with the academic and ethical rules,
- All data, documents, assessments, and results were presented in accordance with the scientific ethical and moral rules,
- All works that were benefitted in the thesis were appropriately cited,
- No alteration was made in the data used,
- Study presented in this thesis is original,

Otherwise, I declare that I accept the loss of all my rights in case any contradiction that may arise against me.

Based on the plagiarism report that was generated on the date of 25/08/2023 by using predetermined filtrations set by Directorate of Institute of Graduate Studies of the Turnitin programme, a plagiarism detection sofware, the similarity index detected was 19 %.

____

Ahmed Rajab AHMED

ABSTRACT

INFLUENCE OF INDUCTION HEATING ON THE PHYSICAL PROPERTIES OF IRON SHEATHED MgB_2
MSC THESIS
AHMED RAJAB AHMED
BOLU ABANT IZZET BAYSAL UNIVERSITY
INSTITUTE OF GRADUATE STUDIES
DEPARTMENT OF PHYSICS
(SUPERVISOR: PROF. DR. MUSTAFA AKDOĞAN)

BOLU, JULY 2023
xiii + 62 pages

In this study, influence of induction heating applied to iron sheathed MgB_2 wires produced by the powder-in-tube (PIT) technique in an argon flow athmosphere on the physical and superconducting properties of the wires was investigated. Laboratory made induction heater system was calibrated via Fluke Ti300+ thermal camera. When the superconductivity properties of MgB_2/Fe wires, which were heat treathed at 900° for 2 minutes with induction heater, were examined, it was observed that the wires had a critical transition temperature of 36.8 K under 0 T magnetic field. It has been concluded that induction heating is an advantageous method in terms of both time and energy efficient when compared to the heat treatments made by the convencional tube furnace.

KEYWORDS: MgB_2/Fe, Wire, Induction Heating, PIT, Superconductivity

ÖZET

DEMİR KILIFLI MgB_2'NİN FİZİKSEL ÖZELLİKLERİNE ENDÜKSİYON ISITMANIN ETKİSİ
YÜKSEK LİSANS TEZİ
AHMED RAJAB AHMED
BOLU ABANT İZZET BAYSAL ÜNİVERSİTESİ
LİSANSÜSTÜ EĞİTİM ENSTİTÜSÜ
FİZİK ANABİLİM DALI

(TEZ DANIŞMANI: PROF. DR. MUSTAFA AKDOĞAN)

BOLU, TEMMUZ - 2023
xiii + 62 sayfa

Bu çalışmada, tüp-içerisinde-toz (TİT) tekniği ile üretilen demir kılıflı MgB_2 tellere argon akış atmosferinde uygulanan endüksiyon ısıtmanın tellerin fiziksel ve süperiletkenlik özelliklerine etkisi araştırıldı. Laboratuvar yapımı endüksiyon ısıtıcısı Fluke Ti300+ termal kamera aracılığı ile kalibre edildi. Endüksiyon ısıtma ile 900° de 2 dakika ısıl işlem gören MgB_2/Fe tellerin süperiletkenlik özellikleri incelendiğinde tellerin 0 T manyetik alan altında 36,8 K kritik geçiş sıcaklığına sahip olduğu gözlendi. Endüksiyon ısıtma yönteminin geleneksel tüp fırın ile yapılan ısıl işlemler ile karşılaştırıldığında hem zaman hem de enerji verimliliği açısından avantajlı bir yöntem olduğu sonucuna ulaşıldı.

ANAHTAR KELİMELER: MgB2/Fe, Tel, Endüksiyon Isıtma, TİT (Tüp İçerisinde Toz), Süperiletkenlik

TABLE OF CONTENTS

LIST OF FIGURES

Page

LIST OF TABLES

Page

LIST OF PICTURES

Page

LIST OF ABBREVIATIONS AND SYMBOLS

PIT	: Powder In Tube
PeIT	: Pellet In Tube
CTFF	: Continuous Tube Filling and Forming
CHPD	: Cold High Pressure Densification
HIP	: High Isostatic Pressure
IMD	: Internal Magnesium Diffusion
EMF	: Electromotive Force
YBCO	: Yittrium Barium Copper Oxide
BSCCO	: Bismuth Strontium Calcium Copper Oxide
MMC	: Metal Matrix Composite
XRD	: X-Ray Diffraction
SEM	: Scanning Electron Microscopy
MRI	: Magnetic Resonance Imaging

ACKNOWLEDGEMENTS

The author wishes to express his deepest gratitude to his supervisor Prof. Dr. Mustafa AKDOĞAN for his guidance, advice, criticism, encouragements, and insight throughout the research.

The author would also like to thank Prof. Dr. Serap SAFRAN and Assoc. Prof. Dr. Murat OLUTAŞ for their suggestions and comments.

1. INTRODUCTION

In view of the increasing demand for energy worldwide, research into more cost-efficient energy production and consumption are inevitable. When switching to industrial applications of a product developed in the field of science, the first thing to consider is the price/performance ratio. Initial production costs and labour costs are included in the price. Based on this idea, we thought about how we can save in terms of both time and cost in superconducting wire production, and we investigated what benefits or gains induction heating can provide for us. Our literature search has shown us that there is no study showing that induction heating was used during the development of MgB_2 wires, and that induction heating will bring us great benefits in terms of time and energy savings (1,2).

When a ferromagnetic material is placed in a time varying magnetic field, an electromotive force (E.M.F.) is induced in the ferromagnetic material. This induced E.M.F. causes eddy currents to flow along a surface of the material. Induction heating occurs when an electromagnetic force field produces and electric current in a metal part. The surface of the part heats due to the resistance to the flow of this electric current. The main factors that control the magnitude and direction of these eddy currents are: 1) the magnitude of the time-varying field, 2) frequency of the time varying magnetic field, 3) the resistivity of the material, 4) the size and shape of the test object, 5) the geometrical shape of the applied field, 6) the location and orientation of the test object to the applied field, 7) the electrical conductivity of the test object, and 8) the magnetic permeability of the test object. A very small change in any one of these can have a marked effect on the eddy current produced. These eddy currents are beneficial in the case of induction heating because they flow inside the material and produce $P=I^2R$ (Watts) losses which causes the material to heat up. So, by controlling the amount of eddy current we can control the temperature of the material.

Induction heating has many advantages, such as environmentally friendly, fast heating speed, fast start-up, high heating efficiency, good controllability, energy savings and high production rates. Induction heating is a technology that respects the working environment because it does not release hot and harmful emissions into the atmosphere. The heat generated within the workpiece by induction provides much higher heating rates than the convection and radiation processes that occur in various types of furnaces. Furnaces contain large amounts of refractory materials that must be heated during start-up, resulting in large thermal inertia. Internal heating in the induction heating process eliminates this problem and allows much faster start-up. When induction heating is not in use, the power supply can be shut off because restarting is so fast. Ovens require continuous power to maintain temperature during delays in processing and to avoid long start-up times. Because heat treatment times are short, induction heating often allows for higher production and lower labour costs. It is widely used in China's automotive industry.

Induction systems are frequently used in industrial applications where precious and non- ferrous metals are used, for processes such as surface hardening, melting, brazing, and welding, annealing, cooking, plastics processing, pyrolysis and heating to fit. In this study, we used an induction coil system with a frequency of 100 kHz, which we purchased and designed in our own laboratory, with parts such as 1 kW maximum power, 500 W power supply, 1.2 kW voltage booster, digital multimeter, aquarium water pump. Induction heating is used in each of the steps of wire production, both stress relief annealing and phase formation annealing.

The MgB_2 superconductor, discovered in 2001, has a high critical transition temperature of 39 K and a simple crystal structure (3). Compared to low-temperature superconductors, it is a great advantage that the MgB_2 superconductor can be efficiently used at temperatures such as 20- 25 K which is also suitable for the need for liquid helium. As a result, the unit cost of operating application equipment can be significantly reduced. The main reasons for using MgB_2 superconductors in applications are the potentially low cost of MgB_2 wire compared to YBCO, BPSCCO/Ag coated conductors or other high-temperature superconductors (4). Due to the many advantages of MgB_2 superconductor, applied research in magnetic resonance imaging (MRI) (5–7), power transmission cables (8,9), wind turbine generators (10–12), superconducting energy storage (Magnetic energy storage, SMES) (13–15), and so on is actively pursued.

Various methods for producing MgB_2 wires can be found in the literature, such as PIT (powder in tube) (16–19), PeIT (pellet in tube) (20), CTFF (continuous tube filling and forming) (21–23), and metal matrix composite (MMC) (24–26). Each method has advantages and disadvantages, but we used the PIT method in this thesis. As for the precursor material, there are two main methods to produce the MgB2 structure: in-situ and ex-situ reactions. In this study (in-situ method was preferred), after preparing the iron sheathed Mg+2B powder mixture obtained by the PIT method, the desired wire diameter was obtained by rolling until it was reduced from 12 mm outer diameter to 1.8 mm outer diameter by using dies with different diameters. Pieces about 10 cm long were cut from the wire. After sealing the two ends of the samples using mechanical press, the resistance-temperature (R-T), current-voltage (I-V), XRD and SEM analyses were performed after annealing the samples at specific temperatures for specific periods of time in the induction heating process under argon flow in the quartz tube.

2. AIM AND SCOPE OF THE STUDY

This study is based on investigating the advantages and disadvantages of using an induction heater, which is a method that can minimize the time and energy consumption experienced during annealing, on iron sheathed MgB_2 wires. The main reasons for choosing an induction heater as a heat treatment tool are its environmental friendliness, high heating speed, fast start-up, high heating efficiency, good controllability, energy saving and high production rates, which makes it a suitable alternative to conventional heating methods.

3. SUPERCONDUCTIVITY

3.1 Discovery of Superconductivity

The first to discover liquid helium was the Dutch physicist Camerling Onnes in 1908. Since liquid helium helped Onnes in his studies learn the properties of materials at temperatures near absolute zero, Onnes discovered a few years later in 1911 that when mercury was cooled to a temperature near absolute zero, the electrical resistance of mercury suddenly became zero, this new state was called superconductivity. An advantage of superconductivity is that there is no energy loss when superconductors are used to transmit DC electrical current.

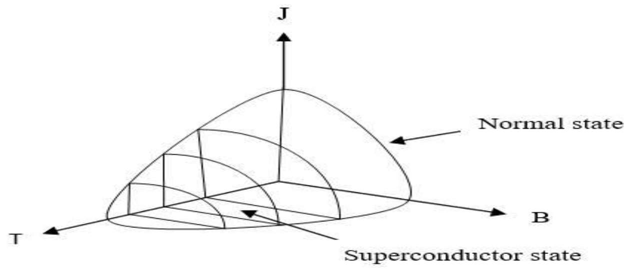

Figure 3.1. Critical boundary between superconducting and normal states.

As it is commonly known, when electricity current passes through a wire, it produces a magnetic field around it. The strength of the magnetic field increases with an increase in the current, and if the magnetic field exceeds a specific level, some materials can lose their superconducting properties and return to their normal state. The highest magnetic field strength at a certain temperature is referred to as the critical magnetic field (B_c). The critical current density (J_c) is the maximum amount of current that a superconductor can carry in its superconducting state, while Tc is the critical temperature at which the superconductor remains in its superconducting state. These three parameters (J_c , B_c , and T_c) are essential properties of any given superconductor, and Figure 1 displays the correlations between them, with each trait dependent on the other two. To maintain the superconducting state, it is crucial to ensure that all three of these material-dependent properties remain below their critical levels.

3.2 Properties of Superconductors

After the discovery of the superconductivity of mercury and a number of other materials, researchers became interested in studying the properties of materials that exhibit superconductivity. One of the most outstanding properties of superconductivity is its ideal conductivity. When a superconductor is cooled to critical temperatures, electric current can flow through the conductor without encountering resistance, meaning there is no loss of energy. This means that an electric current can circulate indefinitely in a closed conductor loop, creating a stable magnetic field that does not decrease with time. Another feature of superconductivity is its ability to exclude magnetic fields, known as the Meissner effect. When a superconductor is placed in a magnetic field, it expels the magnetic field from within. This effect can be used to lift the magnet above the superconductor, as is the case with the recently manufactured Japanese train that uses superconducting technology. A phenomenon known as quantum flux also occurs with superconductors. When a superconductor is in a magnetic field, it allows only discrete amounts of magnetic flux to pass through it. These quantities are expressed in flux units, which are approximately 2.07×10^{-15}T.m^2. This property is essential for many superconducting applications, such as super magnets in MRI machines and particle accelerators. Superconductivity is a quantum phenomenon and as such is described by the laws of quantum mechanics. In a superconductor, electrons form a pair and move through the material as a single unit called a Cooper pair. These pairs are held together by an attractive force called the Cooper pairing force, which is created by the interactions between the electrons and the crystal lattice of the material. This pairing mechanism is still not fully understood and remains an active area of research. Superconductivity is a fascinating phenomenon with many interesting properties and potential applications. The discovery of superconductivity more than a century ago was a major breakthrough, and researchers are still exploring the properties of superconductors and searching for new materials that exhibit this remarkable property.

3.3 Types of Superconductors

3.3.1 Type I Superconductors

Type I superconductors exhibit a number of unique properties, including the Meissner effect, the absence of magnetic flux, and a sharp drop in resistivity at a critical temperature. The absence of magnetic flux in a Type I superconductor is due to the fact that the magnetic field lines are completely repelled by the material, resulting in ideal permeability. However, this property is limited to a certain range of magnetic fields, called the critical field (B_c). Above this field, the superconductivity is destroyed and the magnetic field lines begin to penetrate the material. In a Type I superconductor, the temperature dependence for B_c is approximately the same:

$$B_c(T) \cong B_c(0)[1 - (\frac{T}{T_c})^2] \quad (3.1)$$

$B_c(0)$ represents the magnetic field at (0 K) temperature. Figure 3.2 shows the thermodynamic critical magnetic field value at 0K.

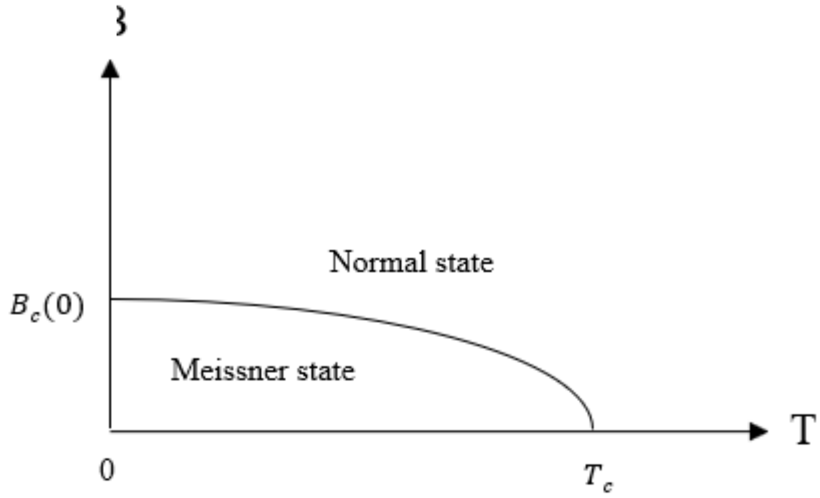

Figure 3.2. The behaviour of type I superconductors, except for Nb, shows a temperature dependence of Bc. All superconducting elements in their pure form show a behaviour of the first type.

As shown in Figure 3.2, the superconductor under the influence of an applied magnetic field Bc is under the influence of Meissner with magnetic susceptibility χ=-1. χ=-1 represents a perfect diamagnetic state and is a measure that weak magnetic fields are completely excluded from a superconductor. One of the disadvantages of Type I superconductors is that they have a relatively low critical field and current density, which limits their practical applications. The best known examples of Type I superconductors are pure metals such as lead and mercury. These materials have relatively simple crystal structures and are well known.

Therefore, they are well suited for studying the fundamental properties of superconductivity.

3.3.2 Type II Superconductors

Type II superconductors differ from type I superconductors in that they have two critical magnetic field values, B_{c1} and B_{c2}. While B_{c1} resembles the magnetic behavior of Type I superconductors, where magnetic flux is completely excluded when the strength of the critical magnetic field is below the critical value, B_{c2} represents magnetic flux that partially penetrates the sample and is not completely displaced. This leads to a vortex state, which is not present in Type I superconductors. In the vortex state, a phase transition from the superconducting state to the normal state takes place above the critical field value B_{c2}.The magnetization curve of a Type II superconductor is shown in Figure 3.3, and it is within the range of $B_{c1}<B<B_{c2}$. The vortex state is characterized by a core surrounded by supercurrents that maintain the magnetic field. The outer magnetic field is concentrated at the center, and the relationship Φ_0= h/2e represents the amount of flow per vortex, where (e) represents the charge of an electron and (h) represents Planck's constant.

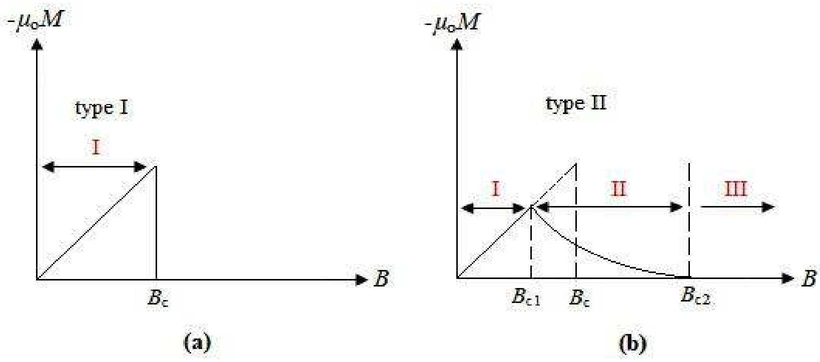

Figure 3.3. The three states of magnetization curves for superconductors of the first and second type are as follows: I: Meissner state II: mixed state III: normal state.

3.4 Fundamental Coefficients of Superconductivity

3.4.1 Critical Temperature (T_c)

The critical temperature (T_c) is one of the most important properties of superconductors. It is defined as the temperature below which the electrical resistance of a material drops to zero. Several factors affect the value of T_c, including the strength of the electron-phonon interaction in the material and the crystal structure of the material. The electron-phonon interaction is responsible for the coupling of electrons in Cooper pairs, which are the building blocks of superconductivity. The stronger the electron-phonon interaction, the higher the temperature. The crystal structure of the material affects the Tc values because the simpler the crystal structure, the higher the T_c value, for example, in metals and alloys. More complex crystal structures tend to disrupt the interactions between electrons and phonons, resulting in a lower T_c value.

3.4.2 Critical Magnetic Field (B_c)

The critical magnetic field (B_c) is the magnetic field that a superconductor can withstand to maintain its superconducting state. Above the B_c value, the metal begins to exhibit normal conduction behavior and loses its superconducting state. Each type of superconductor has different values for the critical magnetic field. For Type I superconductors, above a single critical magnetic field value, there is a sudden loss of superconducting properties. However, in type II superconductors, there are two critical magnetic fields, namely the upper critical field (B_{c2}) and the lower critical field (B_{c1}). In type II superconductors, there is a gradual transition from the superconducting state to the normal conducting state. Above B_{c2}, the superconductor behaves like a normal conductor. Bc1 corresponds to the magnetic field strength at which the vortices begin to penetrate the superconductor, resulting in a gradual transition to the normal conducting state.

3.4.3 Critical Current Density (J_c)

It is the maximum current that the superconductor can withstand without losing its superconducting state. When the current reaches a value greater than the critical current value, the conductor loses its superconducting state and returns to its normal state. The Cooper pairs break down and superconductivity ends at the moment the current rises above the critical current value. The critical current density is the current divided by the cross-sectional area and is characteristic of superconductors. Equation 3.2 represents the current density as a function of the critical magnetic field.

$$\boldsymbol{J_c} \cong \frac{\mathbf{1}}{\mathbf{4\pi\sqrt{3}}} \frac{\boldsymbol{cB_c(0)}}{\boldsymbol{\lambda_L(0)}} \tag{3.2}$$

Where c is the speed of light, λ(0) is the penetration depth, B_c is the magnetic field.

3.5 Fundamental Properties of Superconductors

3.5.1 Zero Resistance

A material becomes a superconductor when its temperature is below the critical temperature (T_c) at which the resistance of the material is zero, allowing all current to flow through it. It was demonstrated that the current in the ends remains constant and does not change over time by measuring the remaining resistance by sending an electric current directly into the loop of a superconductor, and the results showed that the resistance of the superconductor is less than 10^{-26} Ω.m and this value is much smaller than the resistance of copper (10^{-8} Ω.m) at one degree room temperature by 10^{18}. Another feature of superconductors is that the applied magnetic fields are repelled when the superconductor is below a critical temperature at which the applied field is zero, known as the Meissner effect.

3.5.2 Meissner Effect

Meissner effect, the escape of a magnetic field from the interior of a material that is in the process of becoming a superconductor, i.e., losing its resistance to the flow of electric currents, when it is cooled below a certain temperature, called the transition temperature, which is usually near absolute zero. The Meissner effect, a property of all superconductors, was discovered in 1933 by the German physicists Walther Meissner and Robert Ochsenfeld.

When a superconductor in a magnetic field is cooled to the temperature at which it abruptly loses its electrical resistance, all or part of the magnetic field inside the material is repelled. Relatively weak magnetic fields are completely repelled from the interior of all superconductors, except for a surface layer about one-millionth of an inch thick. However, the external magnetic field can be made strong enough to prevent a transition to the superconducting state and to prevent the Meissner effect from occurring.

In general, regions of intermediate magnetic field strength present during cooling produce a partial Meissner effect as the original field in the material is reduced but not completely displaced. Some superconductors designated as type I (e.g., tin and mercury) can be made to exhibit a full Meissner effect by eliminating various chemical impurities and physical imperfections and by selecting the proper geometric shape and size. Other superconductors, referred to as type II (e.g., vanadium and niobium), exhibit only a partial Meissner effect at intermediate magnetic field strengths, regardless of their geometric shape and size. Superconductors of the type II show decreasing magnetic field leakage with increasing magnetic field strength until they abruptly cease to be superconductors in relatively strong magnetic fields.

Figure 3.4 shows a superconductor under an applied magnetic field. The exclusion of the magnetic field from within the superconductor is called the Meissner effect and this exclusion causes magnetic field lines to move closer together on the surface of the superconductor. This means that the magnetic flux inside the superconductor will remain constant, which means that B = 0.

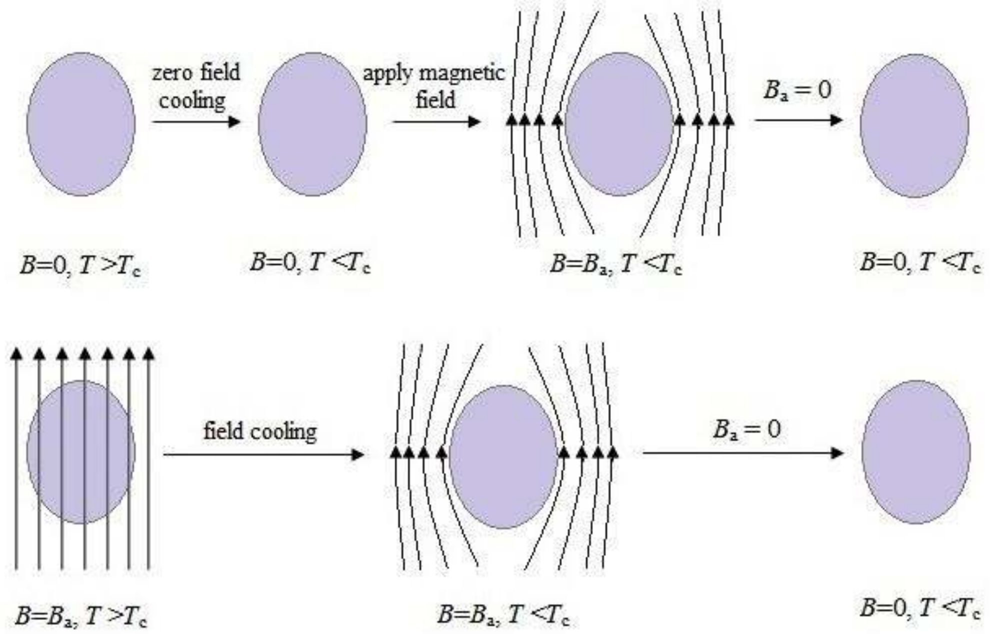

Figure 3.4. This diagram illustrates the Meissner effect for a superconductor under two conditions: zero field-cooled and field-cooled.

3.5.3 London Theory

The London theory was proposed in 1935 by the brothers Fritzou and Heinz. The London theory explains the behavior of superconductors in the presence of a magnetic field because it predicts the Meissner effect, which describes the expulsion of a magnetic field from the interior of a superconductor. To calculate the London equations, we assume that electrons move through the material without resistance under the influence of an electric field that pushes the electrons in a certain direction, which is known as the Lorentz force, as in equation (3.3), taking into account the mass of the electron m, the velocity v, and the time t, as in Newton's second law, equation (3.4). The London equations can be derived as follows:

$$F = m\frac{\partial \vec{v}}{\partial t} \quad (3.3)$$

$$F = -e\vec{E} \quad (3.4)$$

By equating equations (3.3) and (3.4), we get:

$$\frac{\partial \vec{v}}{\partial t} = \frac{-e}{m}\vec{E} \quad (3.5)$$

As it is known, the current is given by the relation:

$$\vec{j} = -en_s\vec{v} \quad (3.6)$$

Where e represents the charge of the electron, n_s represents the density of the number of electrons, and $\vec{v}$ the velocity, which is followed by the London equation. And by taking the derivative of $\vec{j}$ with respect to time t, then substituting the equations into the derivative of $\vec{j}$, we get the first London equation (3.7).

$$\frac{\partial \vec{j}}{\partial t} = \frac{-n_s e^2}{m}\vec{E} \quad (3.7)$$

The initial electric field equation for London was derived, and by applying Faraday's induction law and curling both sides of Equation (3.7), a new result was obtained.

$$\vec{\nabla} \times \vec{j} = -\frac{n_s e^2}{m}\vec{B} \tag{3.8}$$

3.5.4 London Penetration Theory

As we explained earlier in the Meissner effect, the superconductor expels magnetic fields outside its surface at a temperature below its critical temperature. However, scientific observations have shown that the external magnetic field can penetrate into a very thin layer in the outer shell of the material, and its thickness is expressed by the so called London penetration depth and symbolized by the symbol (λ_L) and by using Maxwell's equation ($\vec{\nabla} \times \vec{B} = \mu_0 \vec{J}$) and substituting in the second London equation 3.8 and the application of a curl curl of the magnetic field we obtain:

$$\vec{\nabla} \times \vec{\nabla} \times \vec{B} = \frac{-\mu_0\, n_s e^2}{m}\overrightarrow{B} \tag{3.9}$$

Applying Gauss's law ($\vec{\nabla} . \vec{B} = 0$), we get:

$$\nabla^2 \vec{B} = \frac{\mu_0 n_s e^2}{m}\vec{B} \equiv \frac{\vec{B}}{{\lambda_L}^2} \tag{3.10}$$

We obtain the London equation for penetration depth $\lambda_L = (\frac{m}{\mu_0 n_s e^2})^{\frac{1}{2}}$ where the internal magnetic field decreases to an amount equal to $\frac{1}{e}$ than the external magnetic field applied to the object and since λ_L is very small, we find that the magnetic field is almost non-existent at very small distances. Therefore, Meissner pointed out that there is no magnetic field inside the materials in the superconducting state.

4. MgB_2 SUPERCONDUCTOR

4.1 Discovery, Advantages of MgB_2 Superconductor

Magnesium diboride is a binary compound of magnesium and boron, with a transition temperature of 39 K, that was first discovered as a superconductor by Nagamatsu et al. in 2001 (3) . Since then, the compound MgB_2 has been extensively studied for its unique superconducting properties and potential applications in various fields. MgB_2 has a unique crystal structure consisting of alternating layers of magnesium and boron atoms forming a two-dimensional lattice of boron atoms that serves as the site of electron-phonon coupling. MgB_2 has several advantages over other superconducting materials that make it attractive for various applications. The MgB_2 material has a relatively high temperature compared to conventional low temperature superconductors, which operate at much lower temperatures. MgB_2 is inexpensive, occurs abundantly in nature, and is easily synthesized into ribbons and wires, which is essential for practical applications such as power transmission and magnetic resonance imaging. MgB_2 has a high critical current density (J_c) in high magnetic fields, making it suitable for high-field applications such as magnets for fusion reactors.

4.2 MgB_2 Structure

MgB_2 belongs to the hexagonal crystal system of type A1B2 with space group p6/mmm. It has a lattice structure consisting of layers of magnesium atoms sandwiched between layers of boron atoms. The crystal structure of MgB_2 is unique because it has two different types of bonds. Boron atoms form covalent bonds with their nearest neighbours while magnesium atoms form ionic bonds with boron atoms. The ionic bonding between magnesium and boron atoms is responsible for the high super transition temperature (T_c)(3). XRD analysis showed that the lattice parameters of MgB_2 are a=b=3.081 Å, c=3.52 Å (27), and the unit cell volume is 24.45. Boron and magnesium atoms are aligned together in the form of graphite-like layers in a honeycomb, as shown in Figure 4.1.

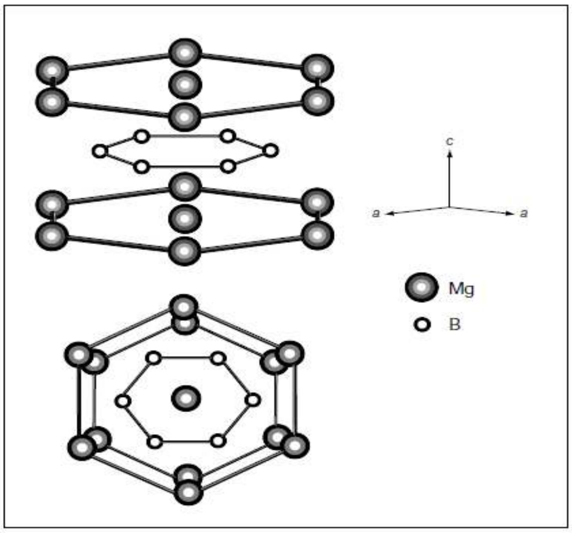

Figure 4.1. The crystal structure MgB_2 superconductor (3).

The distance between one boron atom and another is 1.780 Å and the distance between one magnesium atom and another is 3.084 Å. The strong electron-phonon interactions in the MgB_2 conductor cause the high temperature (T_c), so the MgB_2 compound has a higher temperature than other metals.

4.3 Anisotropy (γ)

Anisotropy is a concept that describes the directional dependence of the electron mass in the material and in different directions, describing the extent to which the electron can move in certain crystal directions more than others. The mass ratio in the a-axis and the c-axis can be used to estimate the anisotropy, which is given by the relationship:

$$\gamma = \sqrt{\frac{mc^*}{ma^*}} \tag{4.1}$$

All of the superconducting parameters of MgB_2 how anisotropy, including the London penetration depth λ, the coherence length ξ, the lower critical field B_{c1} and the upper critical field B_{c2}, as well as for the nature of its electronic band, it also shows anisotropy. In previous studies of the Fermi surface in MgB_2, the π-band is highly isotropic, while the σ-band is highly anisotropic. GL theory can be used to describe the anisotropy of superconducting MgB_2 as follows (28) :

$$\gamma = \sqrt{\frac{m_c^*}{m_{ab}^*}} = \frac{\lambda_c}{\lambda_{ab}} = \frac{\xi_{ab}}{\xi_c} = \frac{B_{c2}^{llab}}{B_{c2}^{llc}} \qquad (4.2)$$

The anisotropic GL theory uses the direction of the external magnetic field (when the magnetic field B and the c axis are parallel) and the effective mass (m*). However, the GL theory does not provide a complete explanation for the anisotropy of the MgB_2 compound in the case of superconductivity (29). In other studies, thin films and shapes were shown. Single-crystal and crystal anisotropy values for the superconducting MgB_2 compound. For example, the anisotropy ratio of the upper critical field Bc_2 ($\gamma = Bc_2^{ab} / Bc_2^{c}$) for MgB_2 single crystals are 2.6 (30). As for the aligned crystal samples, the anisotropy ratio ranges from 1.6 to 1.9 depending on the temperature. The bean model was used to calculate the anisotropy of the critical current density and it was found to be 1.5 (31) .In another study, Angest and others discovered that temperature and magnetic field affect the anisotropy of MgB_2, so that the value of γ decreases from 6 to 2.8 with an increase in temperature from 15 to 35 K. As for the anisotropy of London penetration depth and cohesion length, it is near the transition temperatures in magnetic fields. Low (32).

4.4 Weak Link, Grain Connectivity and Porosity

The superconducting properties of MgB_2 such as critical current density (J_c) and magnetic field dependence are affected by both weak bonds, grain conductivity and porosity. According to (33),(34) the weak bonds in the MgB_2 can be effectively reduced by optimizing the synthesis process and introducing boron nanoparticles and according to their research the critical current density of MgB_2 can be significantly increased by reducing the number of weak bonds. One of the defects affecting the critical current density is the weakness in the grain conductivity, which refers to the degree of bonding between individual grains in a superconducting material. The presence of weak bonds in MgB_2 can lead to a decrease in the critical current density. In their paper, (35) studied the effect of grain contact on the superconducting properties of MgB_2 and found that increasing the grain contact of MgB_2 eads to an improvement in the superconducting properties. As for the porosity, it indicates the presence of voids or pores in the material and the increase in porosity in the MgB_2 works to reduce the critical current density and increase the dependence on the magnetic field.

5. WIRE PRODUCTION METHODS

5.1 PIT (Powder-in-Tube)

The PIT technique is a widely used method for fabricating MgB_2 wires. In this process, a metal tube (Fe, Cu, Nb, Al, Monel, etc.) is filled with Mg and B powders, which are then subjected to high-temperature heat treatment. During this process, the Mg and B powders react to form a superconducting MgB_2 compound that coats the inner surface of the metal tube, resulting in the formation of a wire.

According to (18), the PIT technique has several advantages over other techniques for fabricating MgB_2 wires, such as high critical current density, low fabrication cost, and scalability. The researchers further state that the PIT technique is a versatile method as it can be used to fabricate wires with different diameters and lengths, making it suitable for various applications.

A variant of the PIT technique is the in situ method PIT, in which the superconducting MgB_2 compound is synthesized directly in the metal tube. According to (36), in the in situ method PIT, a metal tube is filled with Mg and B powders and then subjected to high-temperature heat treatment, in which the Mg and B powders react to form the superconducting MgB_2 compound.

The in situ method PIT has several advantages over the ex situ method PIT, as highlighted in (37). In the ex situ method PIT, the superconducting MgB_2 compound is first synthesized in a separate process, and the resulting powder is then placed in a metal tube and subjected to heat treatment. Compared with the in-situ method PIT, the ex-situ method PIT requires a longer heat treatment time, resulting in higher manufacturing costs. In addition, the ex-situ PIT technique may lead to the formation of impurities and defects in the MgB_2 compound, which may reduce the critical current density and mechanical properties.

On the other hand, the in situ PIT technique has some limitations as noted in (38). The authors noted that the in-situ PIT technique may lead to the formation of cracks in the MgB_2 wires due to the high temperature heat treatment process. The researchers suggested that optimizing the heat treatment conditions and using additives could help mitigate these problems and improve the mechanical properties of MgB_2 wires.

5.2 IMD (Internal Magnesium Diffusion)

The IMD technique is a widely used method for fabricating MgB_2 wires. It involves inserting a magnesium rod into the metal sheath and then filling the sheath with boron powder (39), followed by heat treatment at high temperature to cause diffusion of the magnesium into the boron granule and form an MgB_2 composite. According to (40), this technology has many advantages, including high homogeneity of the MgB2 phase, low impurity content, and high critical current density. According to (41), the IMD process is further improved by introducing nanoscale additives such as SiC into the MgB_2 powder. This leads to a significant improvement in the critical current density and improved mechanical properties of the wires.

5.3 CTFF (Continuous Tube Filling and Forming)

CTFF technology (42) is a process for the production of high-performance MgB_2 wires. This process uses a continuous metal tube filled with MgB_2 powder, which is then rolled and drawn. The tube is usually made of niobium, stainless steel or copper, and the MgB_2 powder is hermetically packed inside it before processing. The resulting wire has a uniform microstructure and high current-carrying capacity because the MgB_2 grains are aligned along the wire axis. Superconducting CTFF wires have a critical current density (J_c) of $6\times10^5 A/cm^2$ at a temperature of 10 K and 0 T (21). In a study conducted by Suo et al. it is shown that CTFF technology has many advantages that make it a competitive method for PIT technology. These advantages include ease of fabrication, lower sintering temperature in situ compared to temperatures found ex-situ, and ease of introduction of chemical stimulants.

5.4 CHPD (Cold High Pressure Densification) and HIP (Hot Isostatic Pressure)

Among the many technologies used in the production of MgB_2 wires. Two technologies that have attracted much attention are cold high pressure densification (CHPD) and hot isostatic pressure (HIP). These two processes increase the mass density of MgB_2 and the contact between grains, resulting in a high critical current density (J_c), which is better than the in-situ process PIT for eliminating the porosity of MgB_2 and increasing the contact between grains. The HIP process involves the reaction of MgB_2 powder under high pressure, but for several reasons, the HIP process cannot be applied to long wire samples (43), including a) the small size of the pressure chamber b) argon gas is trapped inside the filament c) limited applied gas pressure (44). The CHPD method can be applied to long wire specimens (45).

5.5 PeIT (Pellet-in-Tube)

Pellet-in-tube (PeIT) technology is a promising technology for the fabrication of MgB_2 wires. In this technique, the initial packing density of Mg+2B powder is increased in situ in an iron sheath. In this process, the metal tube is filled with 50-60% Mg+2B powder, followed by several cold drawing operations and heat treatments in an inert gas atmosphere. This technology provides a high core density with a percentage of porosity that cannot be eliminated. This technique is effective in that it can be applied to long wires with uniform powder filling in the tube (46).

6. INDUCTION HEATING

6.1 History

Induction heating is the generation of heat on a metal surface by eddy currents without the need for physical contact. Induction heating dates back to the early nineteenth century when Faraday discovered the basic principles of electromagnetic induction. Faraday found that an electric current is induced in a conductor when it is subjected to an alternating magnetic field. However, practical applications of this discovery did not come to fruition until the late nineteenth century.

In 1890, the first induction heater was developed by American engineer Edward Allen Colby. Colby used a high-frequency alternating current generator to create an oscillating magnetic field. He demonstrated the heating effect by melting a variety of metals. This invention laid the foundation for further advances in the field of induction heating.

During the twentieth century, induction heating technology evolved into a more advanced induction heating technology with the advent of power electronics and solid-state devices. More recently, induction heating has become a widely used method for many heating processes and industrial procedures.

6.2 The Working Principle of Induction Heating

Induction heating is based on the principle of electromagnetic induction, which states that an electronic circuit generates a high-frequency electromagnetic field in the solenoid coil. The electromagnetic field penetrates the ferromagnetic material to be heated without touching it, and due to the induction of the magnetic field, electric currents called eddy currents are generated in the material, and due to the resistance of the material, the energy is dissipated in the form of heat (47).

6.3 Working Steps and Components of The Induction Heating

The induction heating system includes several main components, including a AC power source needed to operate the circuit, a power transformer to convert alternating current AC to direct current DC, which allows precise control of the induction heater power by increasing or decreasing the value of the direct current, thereby increasing or decreasing the temperature of the workpiece. Then, the DC current is converted to AC alternating current using an IGBT inverter (48), which in turn contains high-frequency transistors, capacitors, and electronic control circuits. The inverter generates a sine or square wave at the frequency required to operate the induction coil, which in turn creates a magnetic field effect on the objects and capacitors placed in the coil, storing energy and discharging it quickly in the coil, allowing the coil to operate more efficiently by supplying high current to the capacitor (49). To prevent the system from overheating and to ensure its safe operation, a cooling system is used that includes a fan and a liquid cooling system. Figure 6.1 shows a diagram of our laboratory made induction heating system.

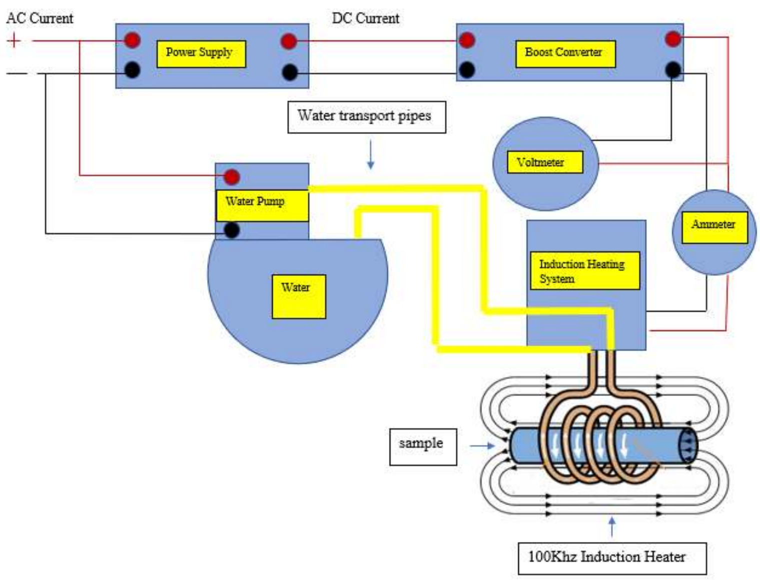

Figure 6.1. Laboratory-made Induction Heating System by Own.

6.4 Eddy Currents

Eddy currents are caused by a change in the magnetic flux emanating from the solenoid coil in the workpiece to be heated; these currents revolve around the magnetic field lines and are rotating and are therefore called eddy currents (47). Eddy currents cause a loss of energy in the workpiece due to the resistance of the eddy currents in the material, and the loss of energy causes an increase in the temperature of the workpiece, which makes them useful for heating metals without contact with them.

6.5 Effect of Power In The Joule Heating Capacity In An Induction Heating System

The Joule phenomenon is defined as the heat generated by the passage of an electric current in conductive materials. The passage of this current causes a loss of energy in the material due to its electrical resistance. The Joule phenomenon is also referred to as the electrical heating phenomenon.

When the electrical power in the induction heater is increased, the rate of conversion of electrical energy to heat in the materials increases, causing the heater to heat up and become hotter. Conversely, when the electrical power is decreased, the conversion rate decreases, so the joule heating decreases.

The capacitance is usually increased by increasing the current, the voltage difference, or both together.

The amount of Joule heating is affected by many other factors, including:

1. Material resistance: the greater the resistance, the greater the Joule heating, and vice versa.

2. The duration of the effect of the magnetic flux on the workpiece: the longer the duration, the greater the Joule heating.

3. Type of conductive material: Conductive materials differ in terms of their electrical resistance, so the magnitude of the joule heating varies (50).

6.6 The Effect of Frequency on Heating Metals Via Induction Heater

The frequency for the induction heating system is chosen according to the type of metal to be heated, as the level of frequency changes depending on some main effects, which include:

1. Skin effect: the skin effect refers to the tendency of the alternating current (AC) to concentrate near the surface of a conductor. At higher frequencies, the skin effect is more pronounced, causing the current to flow mainly through the outer layer of the metal. As a result, heating is concentrated on the surface, leading to rapid heating.

2. Penetration depth: it is the distance at which the induced current in the metal drops to a certain part of its surface value. Higher frequencies result in lower penetration depth, so when using high frequency induction heaters, heating is limited to a thin film, which is useful for applications such as surface hardening or heat treatment.

3. Heating efficiency: the heating efficiency of the induction heater increases as the frequency increases, because higher frequencies cause better coupling between the induction coil and the metal, resulting in better energy transfer and higher heating efficiency.

In general, the choice of frequency for heating metals with an induction heater depends on the depth of heating required, efficiency, power requirements, and the specific properties of the metal to be heated (51).

Table 6.1. Indicates the frequency at which the individual metals are heated with an induction heater.

Material	Frequency Range
Copper	50 kHz - 400 kHz
Aluminum	50 kHz - 400 kHz
Stee	10 kHz - 100 kHz
Iron	10 kHz - 100 kHz
Brass	50 kHz - 400 kHz
Bronze	50 kHz - 400 kHz
Titanium	100 kHz - 400 kHz
Stainless Steel	10 kHz - 100 kHz
Gold	10 kHz - 100 kHz
Silver	10 kHz - 100 kHz

6.7 Inductance In The Solenoid Of An Induction Heater

The inductor is a device that allows to generate a magnetic field in the coil (the coil that generates the magnetic field), which in turn generates an alternating current in the workpiece, and that the inductor is based on Faraday's law of electromagnetic transformation, which states that a change in magnetic flux leads to the generation of an electric current in the conductor in this field and the unit of inductance is the Henry (H).

The relationship between the number of turns n, the magnetic flux Φ_B and the inductance per unit length L/l is:

$$L = \frac{N\Phi_B}{i} = \frac{(nl)(BA)}{i} \qquad (6.1)$$

Where B is the magnetic field and A is the cross-sectional area of the solenoid coil and n is the number of turns of the solenoid for the unit length.

$$B = \mu_o in \tag{6.2}$$

Here μ_0 is the permeability constant equal to ($4\pi\times10^{-7}$ T.m/A), and substituting the value of the magnetic field into the equation gives the equation for the inductance per unit length for a solenoid (52).

$$\frac{L}{l} = \mu_o n^2 A \tag{6.3}$$

6.8 Inductance and Magnetic Field Calculations Of Our Induction Heater System

To calculate the magnetic field (B), magnetic flux (Φ_B), and inductance (L) for a solenoid operatred in a magnetic field with a diameter of 0.06 m, a length of 0.07 m, 7 turns, and a current of 5 amperes, we can use the following formulas:

$$B = \frac{4\pi \times 10^{-7} T.\frac{m}{A} \times 7 \times 5A}{0.07m}$$

$$B = 5 \times 10^{-3} T$$

Let us now calculate the cross-sectional area (A) of the solenoid:

$$A = \pi r^2$$

$$A = \pi \times \left(\frac{0.06}{2}\right)^2$$

$$A = 0.002827\ m^2$$

Then we calculate the magnetic flux (Φ_B):

$$\Phi_B = BA$$

$$\Phi_B = 0.05T \times 0.002827 m^2$$

$$\Phi_B \approx 0.000014135\ webers$$

Finally, let's calculate the induction (L):

$$L = \frac{\mu_o n^2 A}{l}$$

$$L = \frac{4\pi \times 10^{-7} T.m/A \times 7^2 \times 0.002827 m^2}{0.07m}$$

$$L = 0.000253\ H$$

6.9 Induction Heating Applications

The induction heater is widely used in many fields, including medicine, industry and commerce, because the induction heating process is clean and free from environmental pollutants, and its high operating speed and good controllability make it a suitable alternative to conventional heating methods. In medicine, for example, the induction heater has been used for local high-temperature treatment of tumours by heating the tissue directly by the eddy currents generated in the cylindrical implants (53), and it has also been used to remove liver tumours (54). In industry, the induction heater has been used to heat various metal objects using HTS superconducting magnets (55). The induction heater has also been used in the processing of steel and metals for heat treatment (56) and in surface hardening and welding applications (57). As for the commercial aspect, the induction heater can be used as an alternative to the conventional oven in cooking food (58) and (59).

6.10 Emissitivy Values for Metals

Emissivity is a measure of an object's ability to emit infrared energy. The energy emitted indicates the body temperature. The emissivity can take a value between 0 (shiny mirror) and 1.0 (black body). Most organic, coated, or anodized surfaces have an emissivity of about 0.95. In our studies, we used a Fluke Ti300+ thermal imaging camera, shown in picture 6.7, to measure the surface temperature of all our samples. Table 6.1 shows the emissivity values for different elements under different conditions (https://www.flukeprocessinstruments.com/en-us/service-and-support/knowledge-center/infrared-technology/emissivity-metals).

Picture 6.1. Fluke Ti300+ thermal camera.

Table 6.2. Emissitivy values for various metals.

Material	Emissivity Values		
	1.0µm	1.6µm	8-14µm
Aluminium			
Unoxidized	0.1-0.2	0.02-0.2	not recommended
Oxidized	0.4	0.4	0.2-0.4
Alloy A3003			
Oxidized	not recommended	0.4	0.3
Roughened	0.2-0.8	0.2-0.6	0.1-0.3
Polished	0.1-0.2	0.02-0.1	not recommended
Brass			
Polished	0.8-0.95	0.01-0.05	not recommended
Burnished	not recommended	not recommended	0.3
Oxidized	0.6	0.6	0.5
Chromium	0.4	0.4	not recommended
Copper			
Polished	not recommended	0.03	not recommended
Roughened	not recommended	0.05-0.2	not recommended
Oxidized	0.2-0.8	0.2-0.9	0.4-0.8
Electrical Terminal Blocks	not recommended	not recommended	0.6
Gold	0.3	0.01-0.1	not recommended
Haynes			
Alloy	0.5-0.9	0.6-0.9	0.3-0.8
Inconel			
Oxidized	0.4-0.9	0.6-0.9	0.7-.95
Sandblasted	0.3-0.4	0.3-0.6	0.3-0.6
Electropolished	0.2-0.5	0.25	0.15
Iron			
Oxidized	0.4-0.8	0.5-0.9	0.5-0.9
Unoxidized	0.35	0.1-0.3	not recommended
Rusted	not recommended	0.6-0.9	0.5-0.7
Molten	0.35	0.4-0.6	not recommended
Iron, Cast			
Oxidized	0.7-0.9	0.7-0.9	0.6-0.95
Unoxidized	0.35	0.3	0.2
Molten	0.35	0.3-0.4	0.2-0.3
Iron, Wrought			
Dull	0.9	0.9	0.9
Lead			
Polished	0.35	0.05-0.2	not recommended
Rough	0.65	0.6	0.4
Oxidized	not recommended	0.3-0.7	0.2-0.6
Magnesium	0.3-0.8	0.05-0.3	not recommended

7. EXPERIMENTAL DETAILS

7.1 Preparation of in-situ Mg+2B Powder

Magnesium (pvz) powder with a purity of 99% and a particle size of 74-149 μm and amorphous boron (pvz) powder with a purity of 95-97% and a particle size of less than one μm were used to prepare the primary Mg+2B powder. Based on the stoichiometry of the reactants, we calculated the mass of magnesium and boron required to form 20 g of the Mg+2B mixture; the mass of magnesium is 10.5841 g and the mass of boron is 9.4152 g. The Mg+2B mixture was ground with garnet balls of different sizes (mass ratio 4:1) for 3 hours in the ball mill shown in Figure 7.1. The Mg+2B powder was stored in a bottle covered with parafilm in an argon atmosphere to protect the powder from moisture for as long as possible.

Picture 7.1. Ball milling machine.

7.2 Filling Iron Tube with Mg+2B Powder (PIT)

To make the MgB_2/Fe tube, we used an iron sheath with an outer diameter of 12 mm, an inner diameter of 9 mm, a thickness of 1.5 mm, and a length of 20 cm. Then we close the base of the sheath with aluminum foil, length of 1.5 cm, then we gradually empty the Mg +2B powder into the iron sheath so that the powder reaches the top of the sheath and then close the top with aluminum also with a length of 3 cm, the mass of Mg +2B powder used to fill the iron sheath is 14.503 g. The rest of the unused mixture is 5.4963 g. The iron sheath used to make the MgB_2/Fe wire is kept in a glove box tightly covered with parafilm (Figure 7.2).

Picture 7.2. Iron sheath with Mg +2B powder inside.

7.3 Wire Making Steps

The superconducting MgB_2/Fe wires were fabricated in situ using the PIT techniques for stoichiometric Mg + 2B powder ratios, and then the iron sheath undergoes a series of drawing and rolling processes to reduce its diameter from 12 mm to 1 mm, resulting in a natural increase in the length of the wire. Figure 7.3 shows the tools and equipment used to produce MgB_2/Fe wires. Table 7.1 shows the drawing steps for the MgB_2/Fe wire.

Table 7.1. Drawing steps for the MgB_2/Fe wire.

Steps	Diameters of dies	steps	Diameters of dies
1	11.30 mm	30	5.30mm
2	11.00 mm	31	5.15mm
3	10.80 mm	32	5.00mm
4	10.65 mm	33	4.85 mm
5	10.50 mm	34	4.70 mm
6	10.30 mm	35	4.50 mm
7	10.00 mm	36	4.45 mm
8	9.80 mm	37	4.30 mm
9	9.50 mm	38	4.25 mm
10	9.20 mm	39	4.10 mm
11	9.10 mm	40	3.95 mm
12	8.90 mm	41	3.85 mm
13	8.60 mm	42	3.75 mm
14	8.50 mm	43	3.72 mm
15	8.35 mm	44	3.57 mm
16	8.20 mm	45	3.43 mm
17	8.00 mm	46	3.27 mm
18	7.75 mm	47	3.12 mm
19	7.60 mm	48	3.00 mm
20	7.40 mm	49	2.85 mm
21	7.20 mm	50	2.71 mm
22	6.90 mm	51	2.64 mm
23	6.70 mm	52	2.50 mm
24	6.50 mm	53	2.38 mm
25	6.30 mm	54	2.21 mm
26	6.20 mm	55	2.10 mm
27	6.10 mm	56	2.00 mm
28	5.90 mm	57	1.90 mm
29	5.50 mm	58	1.80 mm

a) Drawing machine (17 meters)

b) Rolling machine (from 1 mm to 15 mm)

c) Tungsten Carbide Dies (inner diameters from 0.5 mm to 15 mm)

Picture 7.3. In the production of wires, machines such as groove rolling, long wire drawing and dies with different inner diameters are used.

7.4 Closing Both Ends of The Wires

Before heat treating our samples, we need to protect the MgB_2 inside our wires from leaking Mg during heat treatment by sealing the two ends of each sample of our superconducting wires, pressing the two ends of each sample with a pressure of 5 bar using the pressing machine shown in Figure 7.4.

Picture 7.4. Mechanical press.

7.5 Heat Treatment Process

Heat treatment of MgB_2 nanowires was performed once during wire drawing and several times after drawing. All heat treatment processes were performed using the induction heater shown in Picture 7.5. During the first heat treatment process the MgB_2 wires were heated to 500 °C for 2 minutes per 1 cm. This process facilitates the drawing of the wires and protects them from breakage. Of course, attempts have been made to obtain phase transitions at many temperatures before the above values (from 650 to 1000 °C), but since the optimum superconductor transition temperatures have been observed after 800 °C. After drawing, four samples of 10 cm long MgB2 wires were heated to temperatures of 800-850-900-950 °C for two minutes under argon flow using an induction heater (Figure 7.6). At this stage, we determined the appropriate temperature based on the R-T measurement results, this temperature was 900 °C. So, in the third heat treatment step, we heat treated three more samples at 900 °C for 5,10, and 20 minutes respectively. The induction heater was chosen as the tool for heat treating of the MgB_2 wire instead of the tube furnace because the samples heat treated with the induction heater seem to have greater flexibility than the wires heat treated with the tube furnace, while maintaining the same superconducting properties in a record time of a few minutes compared to the tube furnace, which take several hours.

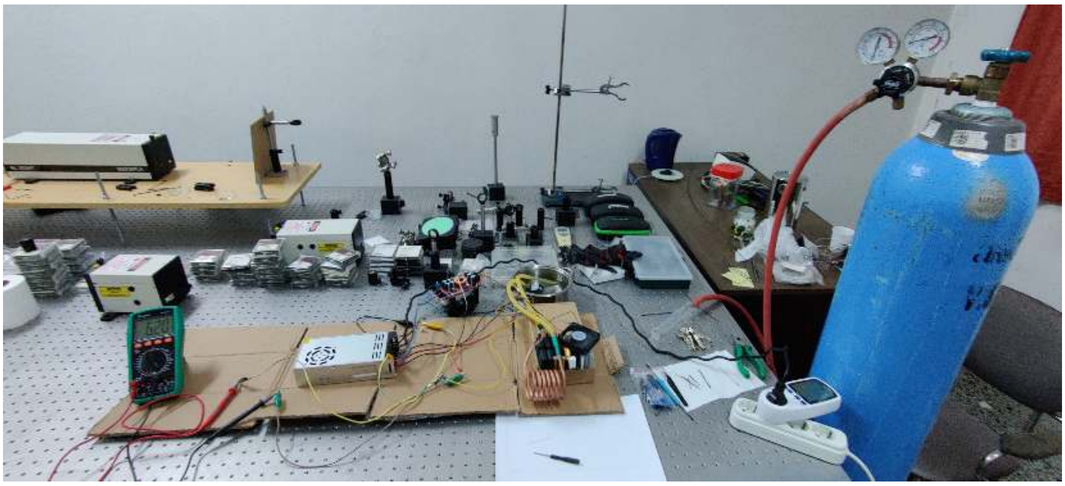

Picture 7.5. 1 kW induction heating system.

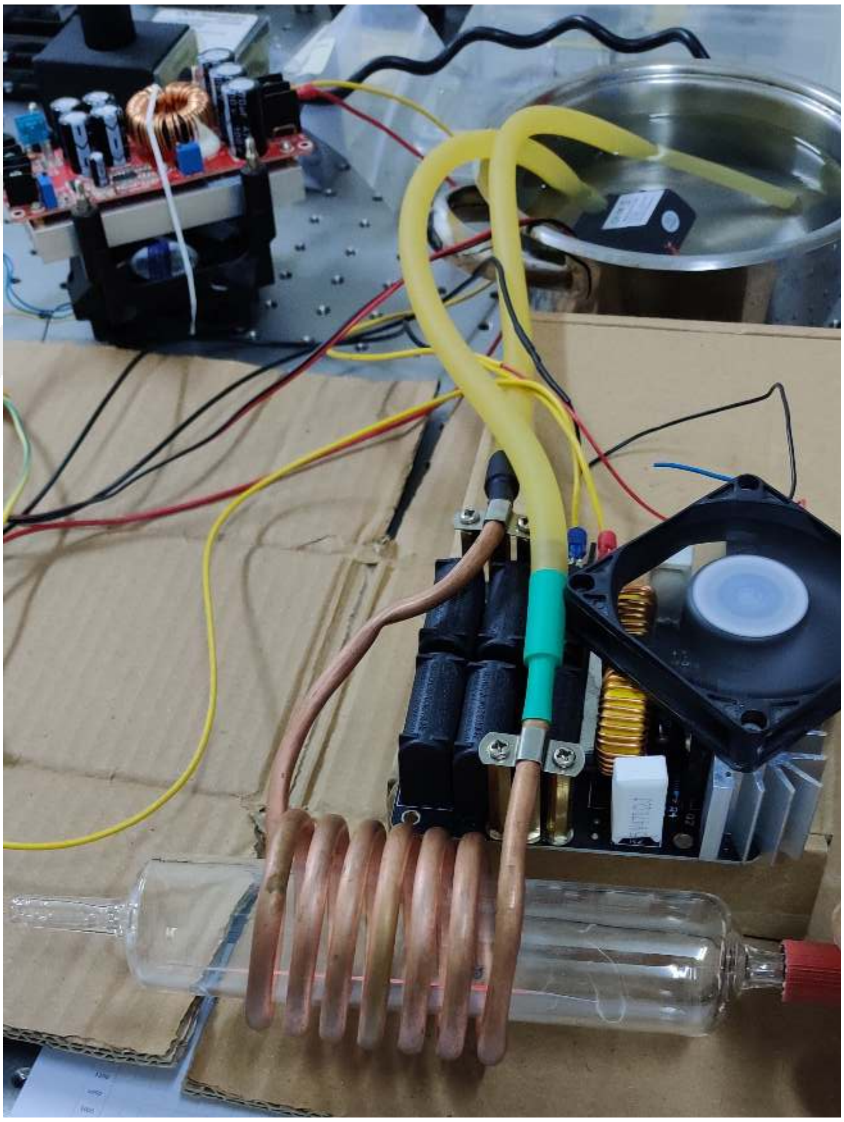

Picture 7.6. MgB_2/Fe wire with a diameter of 1.8 mm, heat treated at a temperature of 900 degrees Celsius for two minutes under argon athmosphere.

7.6 X-Ray Analysis

X-ray diffraction is an important application in the qualitative and quantitative analysis of powders, thin films, and single crystals. Phase composition analysis of MgB_2/Fe wires was performed by grinding half ot the wire as a longitudinal section for XRD analysis from 5 to 90 degrees with 3°/min scanning rate (XRD beam acceleration at 36kV/26mA). Picture 7.7 shows the use of a Rigaku MultiFlex+ diffractometer (with CuK_α radiation, λ = 1.5418 Å) to perform X-ray diffraction.

Picture 7.7. X-ray diffractometer for crystal structure analysis.

7.7 Scanning Electron Microscopy (SEM) Analysis

To observe objects too small for a normal microscope, scientists often use scanning electron microscopy (SEM), in which a beam of electrons is directed at a sample in a vacuum chamber using magnetic lenses. As the electrons interact with the sample's atoms, they reflect beams with unique properties for each atom. This produces a detailed, magnified 3D image in black and white that reveals information about the crystal structure, chemical composition and grain orientation of the surface. In this case, the surface of superconducting MgB_2/Fe wires was analyzed using a scanning electron microscope (JEOL 6390-LV), as shown in Picture 7.8, and SEM images were acquired.

Picture 7.8. (SEM) Scanning electron microscope (JEOL 6390-LV).

7.8 Electrical Characterization of The Samples

The four-point probe method is used to determine the electrical transport properties of materials like the electrical conductivity, the resistivity, the hall constant, the charge carrier concentration and the charge carrier mobility. The four-probe technique has been used to measure resistance as a function of temperature (R-T) and current as a function of voltage to determine the temperature at which resistance falls to zero, usually referred to as the critical temperature (T_c), and to determine the critical current density (J_c) values of samples, respectively. The outer probes of the technique are connected directly to the current source, while the inner probes are connected to a voltmeter. The probes are soldered to the MgB_2/Fe wire samples with a mixture of 60 percent tin and 40 percent lead. Four samples were simultaneously attached to the sample holder of the helium-gas contact cryostat system (Figure 7.9) using GE varnish, and the other ends of the soldered copper wires were soldered to the measurement tips. The R-T measurement was performed by applying 100 mA current to each sample, with a heating rate of 2°/min. in the temperature range of 10-50 K. I-V measurements of the samples were made in the same system by applying a current in 0.05 A steps ranging from 0-1 A, while the temperature was fixed at 25 K. The value for the critical current density (J_c) was determined by measuring the voltage-current relationship, using 1 V/cm as the criterion. The cryostat system can be operated with a maximum DC current of 1 A and a maximum magnetic field of 7 T.

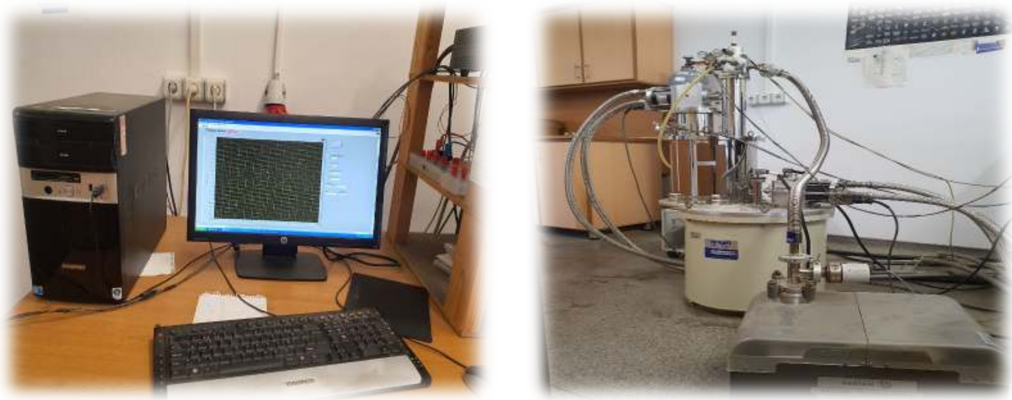

Picture 7.9. 7 T 2.2 K cryostat system (Cryo Industries) for characterization of superconducting properties of samples.

8. RESULTS AND DISCUSSION

In this study, in-situ MgB_2/Fe wires were fabricated by the PIT method and annealed by induction heating. Electrical (R-T and I-V) and structural characterizations (XRD and SEM) of the obtained samples were performed. The following subsections contain the results and comments.

8.1 Magnetoresistivity Measurements

In Figures 8.1 to 8.7, the resistivity behavior of the iron-sheathed MgB2 material prepared by the in situ PIT method was investigated under the magnetic field (0, 1 and 3 T) of samples treated with induction heating (under argon flow) at 800 to 950 degrees Celsius for certain periods of time. Samples about 2-2.5 cm long were cut from the center of our wires, which were originally 10 cm long and had an outer diameter of 1.8 mm, with both ends closed. Insulated copper wires were soldered to these samples using the four-point contact method. For the resistivity-temperature measurements, the samples were placed in the sample holder of the helium gas contact cryostat system. For the R-T measurements, a DC current of 100 mA was applied from the two outer ends of the four-point contact. Then, the distance between the voltage terminals of the samples and the sample diameters were measured with a caliper and the resistance temperature curves were determined by inserting them into the resistivity formula.

All results obtained from the resistivity vs. temperature curves of the samples are shown in Table 8.1. When comparing the samples heat treated at different temperatures for the same time, the highest critical transition temperature (36.8 K) was observed for the sample at 900 °C for 2 minutes (sample C) under self magnetic field (0T). However when comparing the resistivity values of these samples the one with the lowest resistivity is at 800 °C for 2 minutes (36.99 μΩ·cm). Of course, it is not possible to determine the best with the critical temperature alone, but considering these values, the results of heat treatment at 900 °C for 5, 10 and 20 minutes were compared with the results of heat treatment in 2 minutes. When samples C, D, E and F, heat-treated at the same temperature for different lengths of time, were compared with each other, the highest critical transition temperature was found for samples C and D.

Examining the magnetoresistance measurements in Figures 8.1 through 8.7, it can be seen that as the magnetic field increases, the critical transition temperatures decrease as expected. When comparing all samples, it was found that there are slight differences in the critical transition temperatures that can be considered a margin for experimental error.

Table 8.1. Heat-treated samples at different temperatures and different times and the level of resistance of each sample with critical temperatures at magnetic fields (0T, 1T, 3T).

Samples	**Heat treatment temperature(°C)**	**Time (minute)**	**Critical temperature T_c (K), (0T)**	**Resistivity ρ(μΩ·cm) (0T)**	**Critical temperature T_c (K), (1T)**	**Resistivity ρ(μΩ·cm) (1T)**	**Critical temperature T_c (K), (3T)**	**Resistivity ρ(μΩ·cm) (3T)**
A	800	2	36.4	36.99 at 38K	32.4	39.91 at 34.65K	25.2	53.91 at 28.23K
B	850	2	36.1	121.43 at 37.99K	32.5	120.67 at 67 at 34.74K	25.1	119.06 at 28.65K
C	900	2	36.8	104.22 at 38.01K	32.7	103.13 at 34.92K	25.0	103.46 at 28.64K
D	900	5	36.8	107.99 at 38.15K	33.1	107.16 at 35.05K	25.5	103.02 at 28.74K
E	900	10	36.6	126.78 at 37.86K	32.3	125.55 at 34.68K	25.0	124.64 28.77K
F	900	20	36.2	77.96 at 37.87K	32.5	79.22 at 34.76K	25.3	88.39 at 28.86K
G	950	2	36.6	71.25 at 37.99K	32.8	72.27 at 34.80K	26.1	78.12 at 28.68K

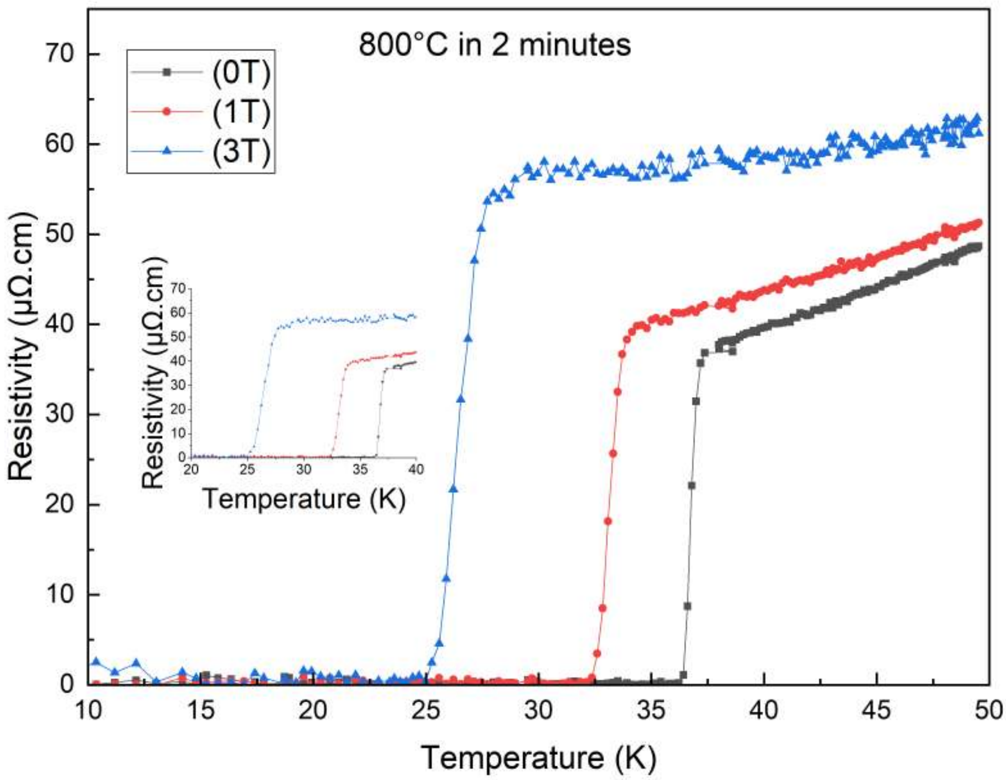

Figure 8.1. Magnetoresistivity measurement of sample A.

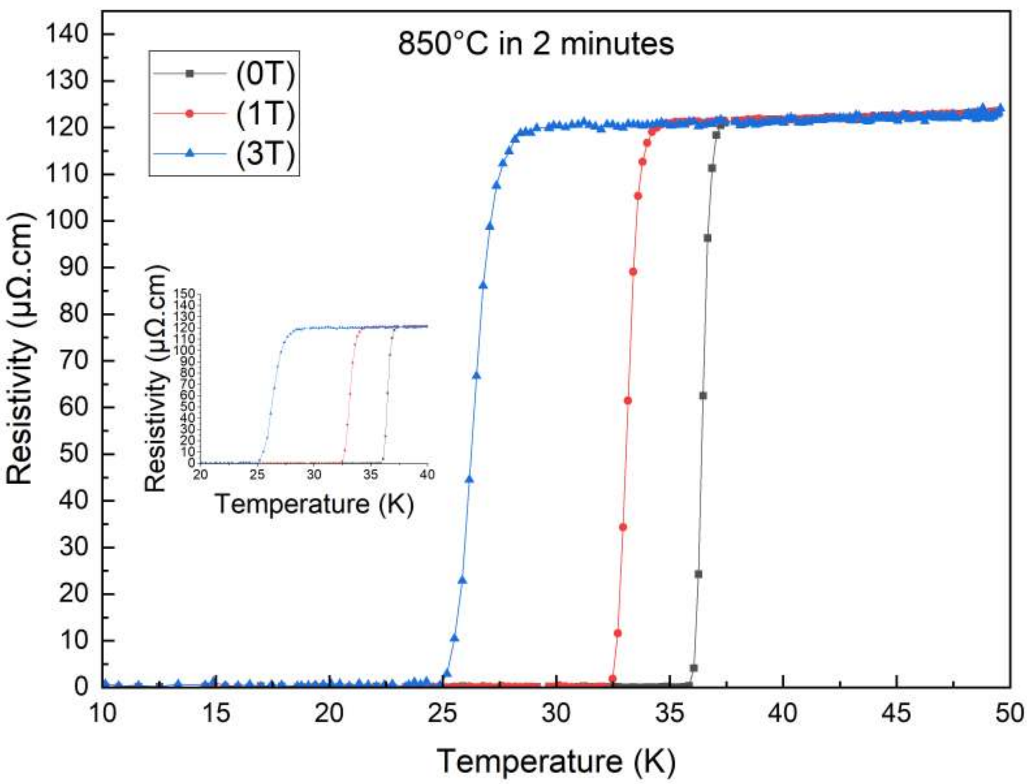

Figure 8.2. Magnetoresistivity measurement of sample B.

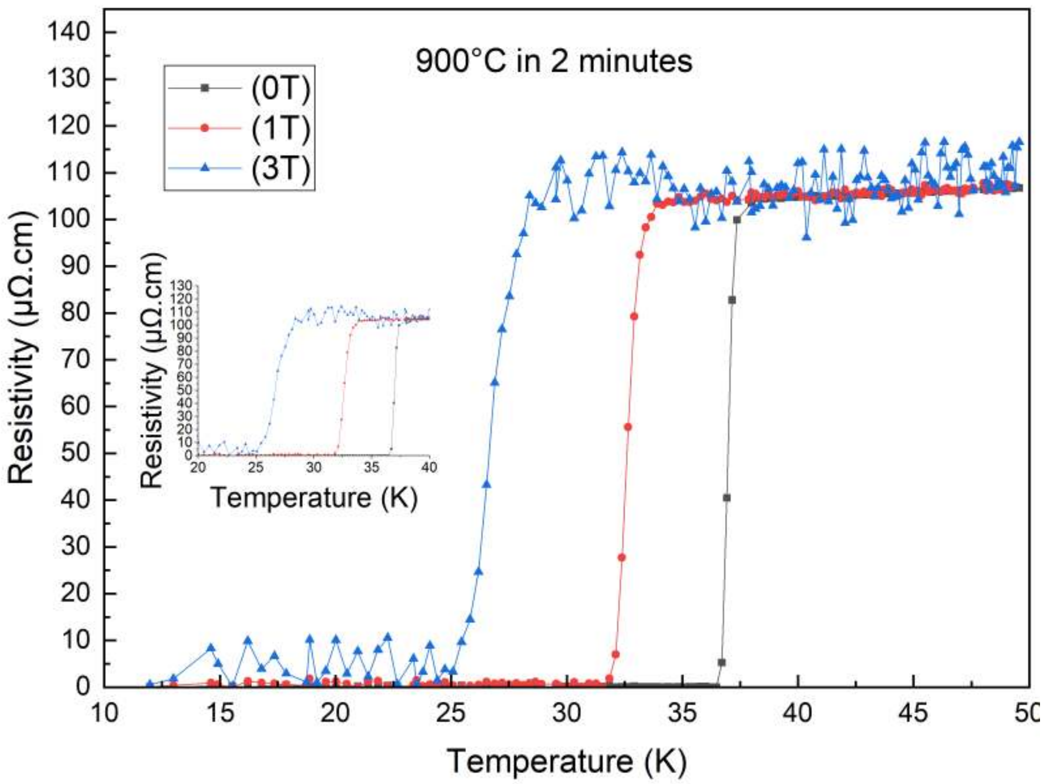

Figure 8.3. Magnetoresistivity measurement of sample C.

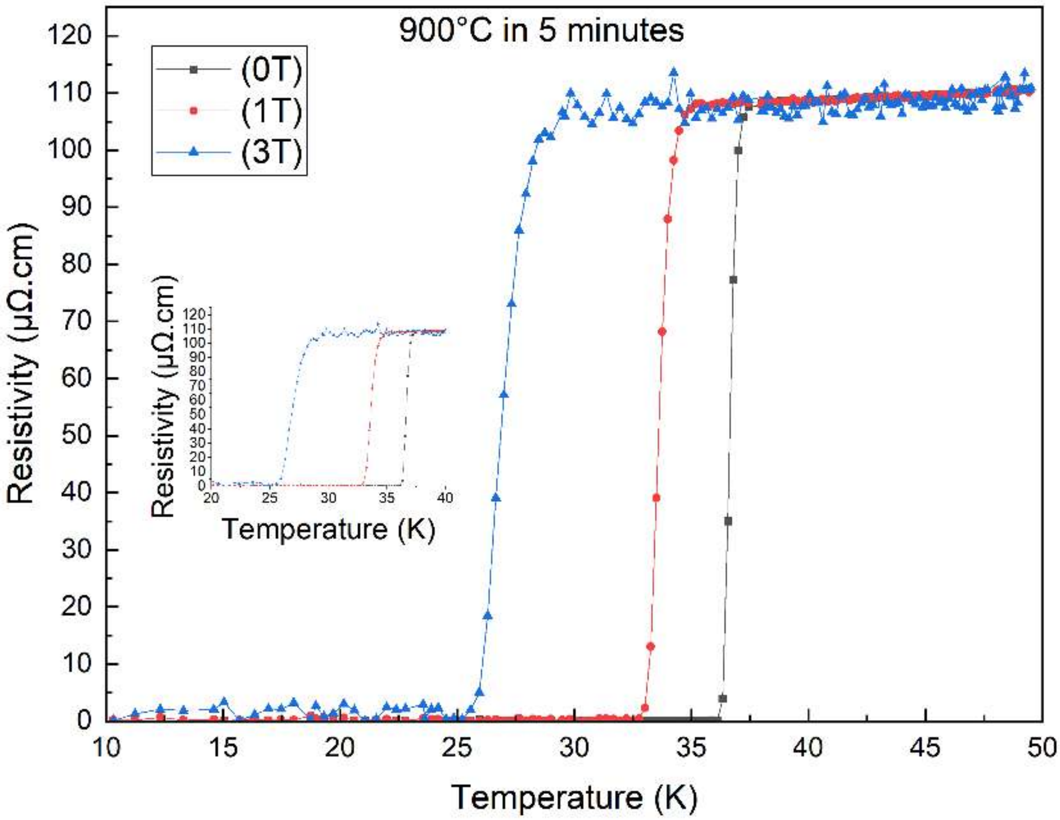

Figure 8.4. Magnetoresistivity measurement of sample D.

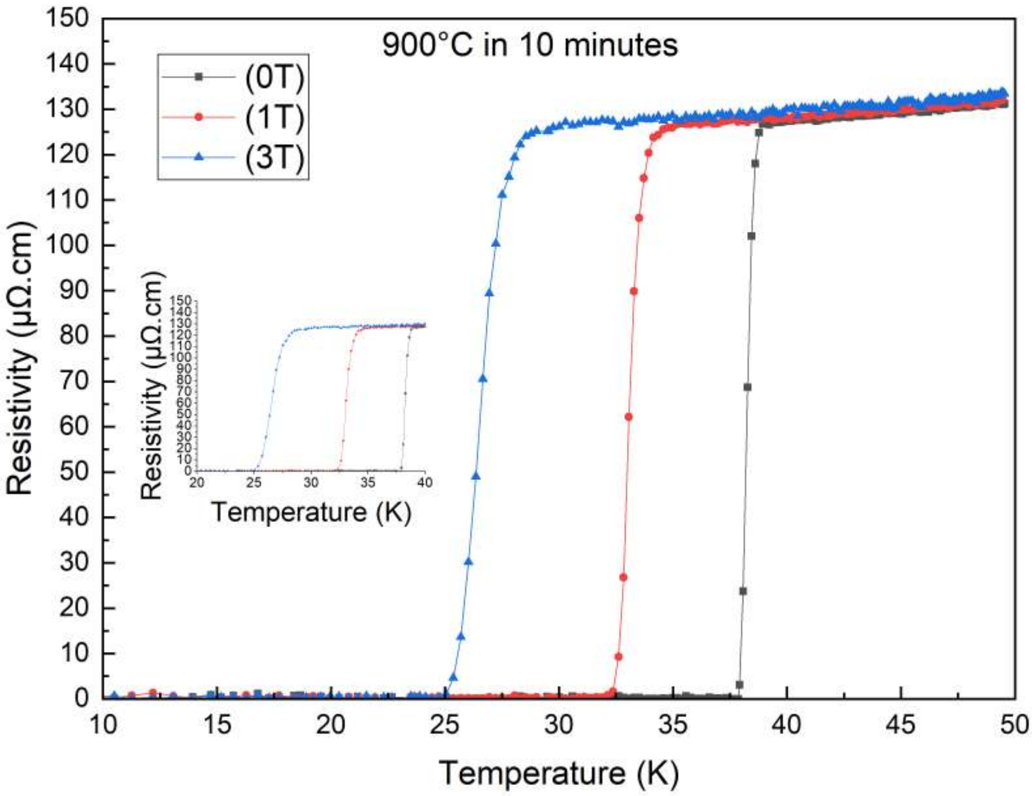

Figure 8.5. Magnetoresistivity measurement of sample E.

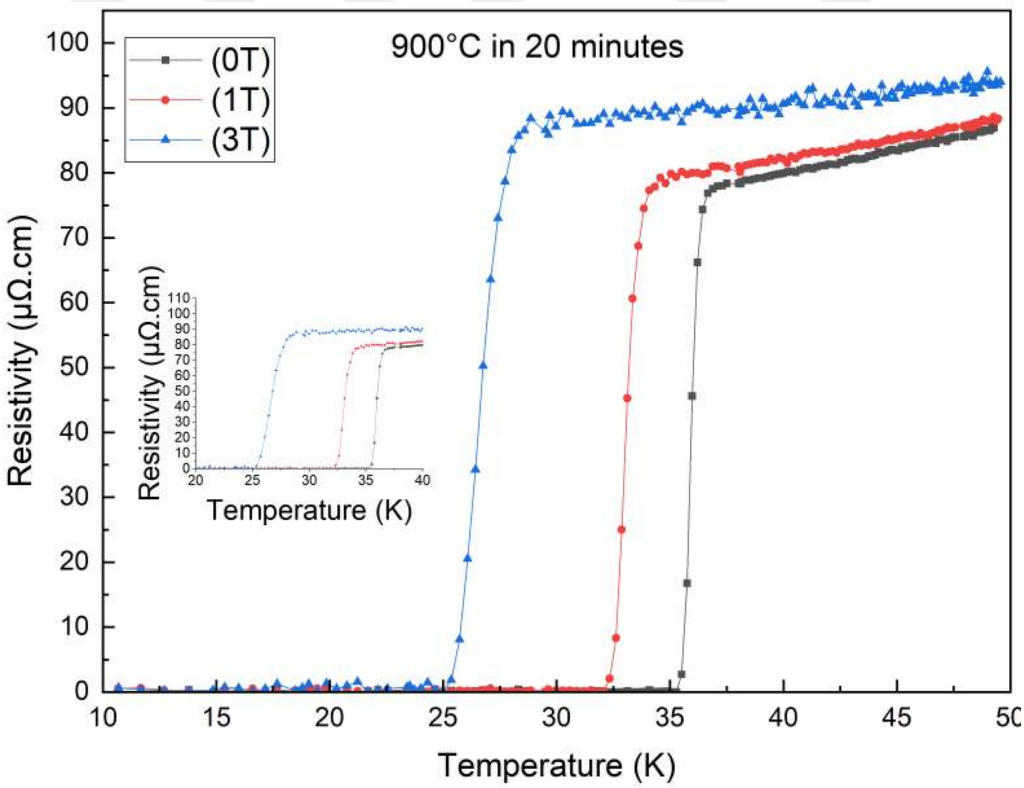

Figure 8.6. Magnetoresistivity measurement of sample F.

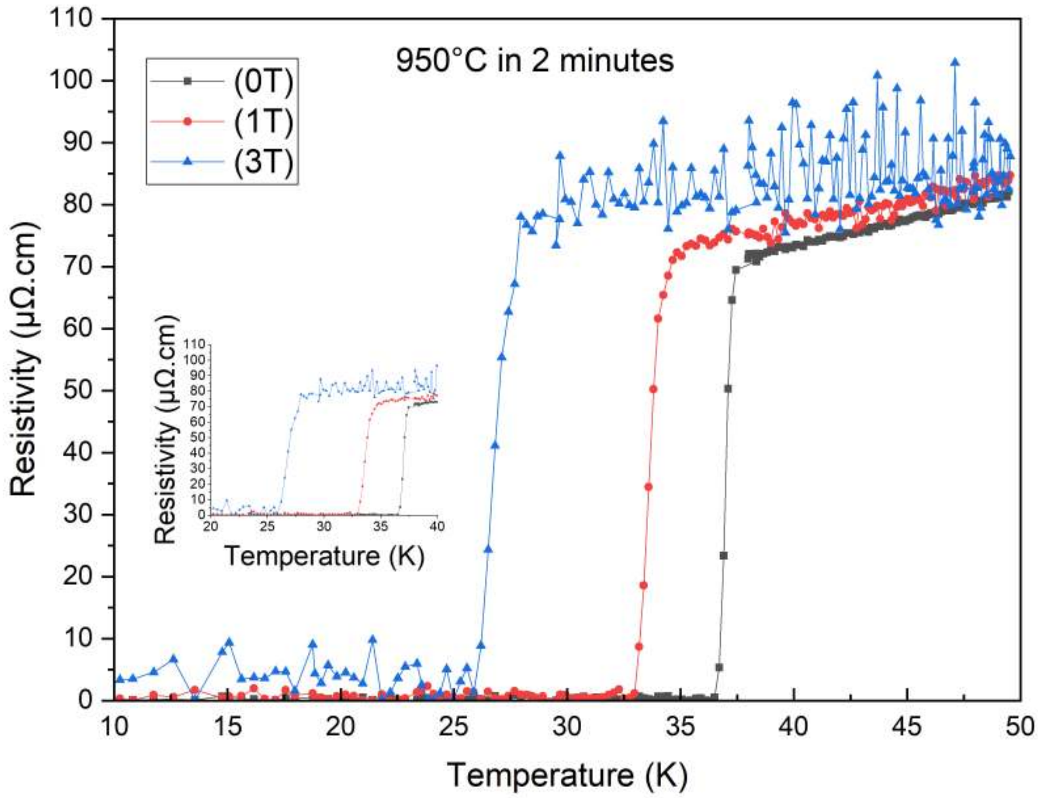

Figure 8.7. Magnetoresistivity measurement of sample G.

Figures 8.8 and 8.9 show the curve of resistivity versus temperature of the samples heat treated at 900 °C for different times and the curve of resistivity versus temperature of the samples heat treated for 2 minutes at different temperatures, respectively. Looking at Figure 8.8 and 8.9, although the values are very close, you can see the differences between them in the inset placed in the graph. In Figure 8.8, there is a jump in the data between 37 and 38 K in the measurement for the red colored sample at 900 °C 5 minutes. This jump is an occasional error of the measurement system.

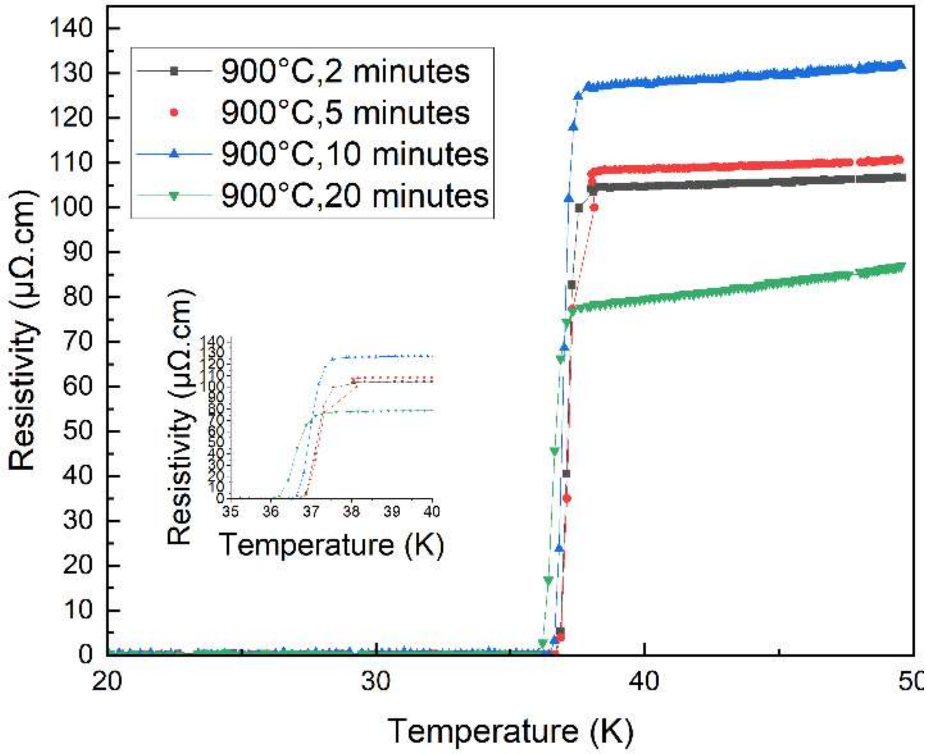

Figure 8.8. Temperature versus resistivity curve of samples that were heat treated at 900 °C for various times under self magnetic field.

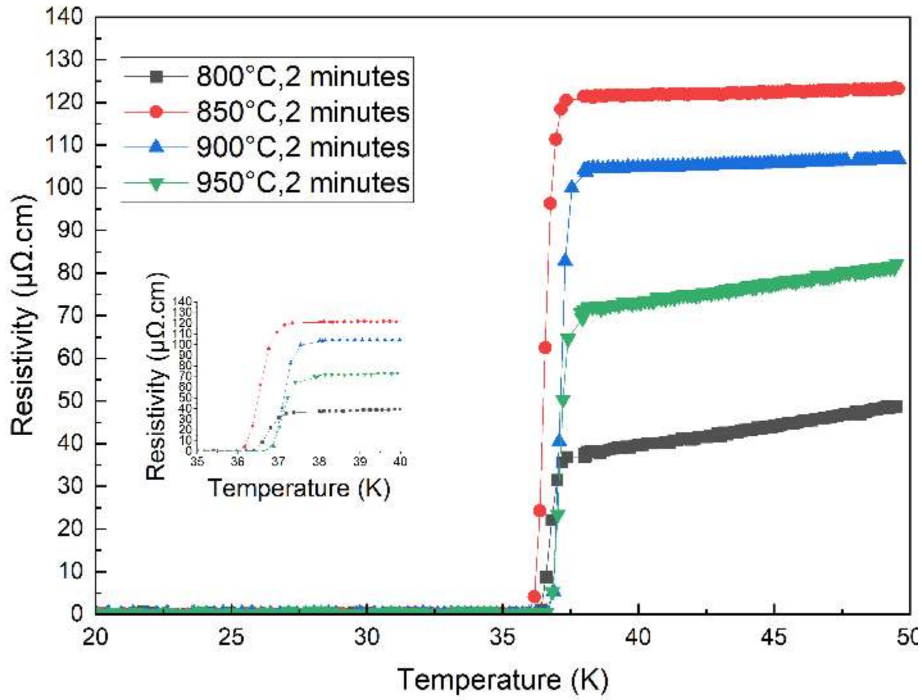

Figure 8.9. Temperature versus resistivity curve of samples that treated at different temperatures under self magnetic field for the same period of time.

8.2 Current-Voltage (I-V) Measurements

Under normal conditions, making I-V measurements with high-current supplies in the liquid helium environment provides more advantageous and reliable results. However, the increasing cost of liquid helium and the impracticalities lead us to the current possibilities. The power source connected to our cryostat system can supply a maximum of 1 A of current. For this reason, we make our measurements by setting our temperature controller to a value as close as possible to the critical temperature. Based on our previous experience, we set the temperature controller to 25 K. After waiting about 1 hour for this temperature value to settle, we started making I-V measurements under the magnetic field. The reason we apply a magnetic field is so that we can see the transition from the superconductor to the normal state. Otherwise, since the sample carries a very high current, it is not possible to observe the transition from the superconductor to the normal conductor state. In our cryostat system, a maximum magnetic field of 7T can be applied. The applied magnetic field is perpendicular to the longitudinal section of the sample. The measurement results are shown in Figure 8.10 for different temperatures and similar times and in Figure 8.11 for the same temperature and different times. The data from these measurements are shown in Table 8.2. The values given in the table for the engineering critical current density were calculated from the I-V curves using the 1 μV/cm criterion and taking into account the sample sizes.

As you can see from Table 8.2, all samples have different engineering critical current densities. Noti that for samples C and F, "no transition" is indicated. This is because the current we have specified is not sufficient to return the sample to the normal state. Moreover, this situation shows that samples C and F have higher current carrying capacity. In our future studies, we plan to investigate the current densities of these samples in detail by making measurements in the liquid helium environment in Poland.

Comparing the values calculated from the I-V measurements of the samples treated for 2 minutes at different temperatures, we can say that the C sample prepared at 900 degrees, where no transition was observed, is the best sample. However, when comparing samples heat treated at the same temperature and at different times, it is not possible to say which sample is the best. The reason for this is that no transition can be observed in both the C and F samples.

Table 8.2. Shows the heat treatment temperatures, times and J_e values of the samples.

sample	Temperature(°C)	Time(minutes)	J_e (A/cm²),(3T)
A	800	2	26.34
B	850	2	11.79
C	900	2	No transtion
D	900	5	25.56
E	900	10	21.23
F	900	20	No transtion
G	950	2	32.63

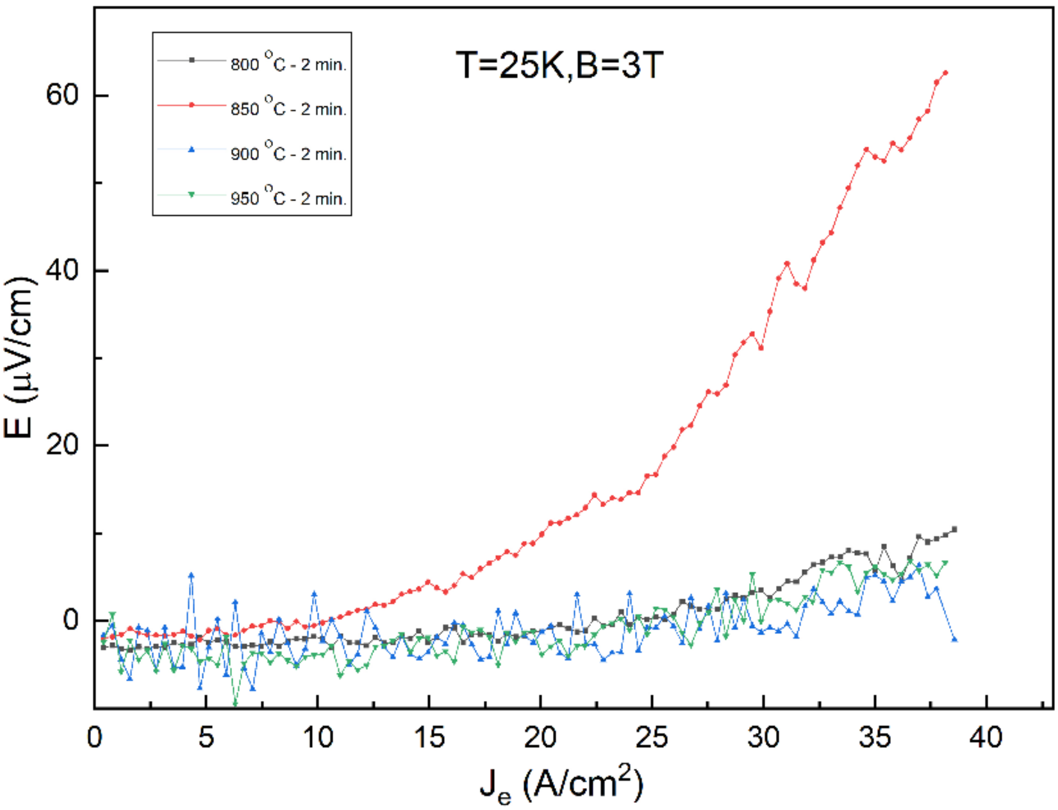

Figure 8.10. J_e vs. E curve of samples sintered at 800, 850, 900 and 950 °C for 2 minutes.

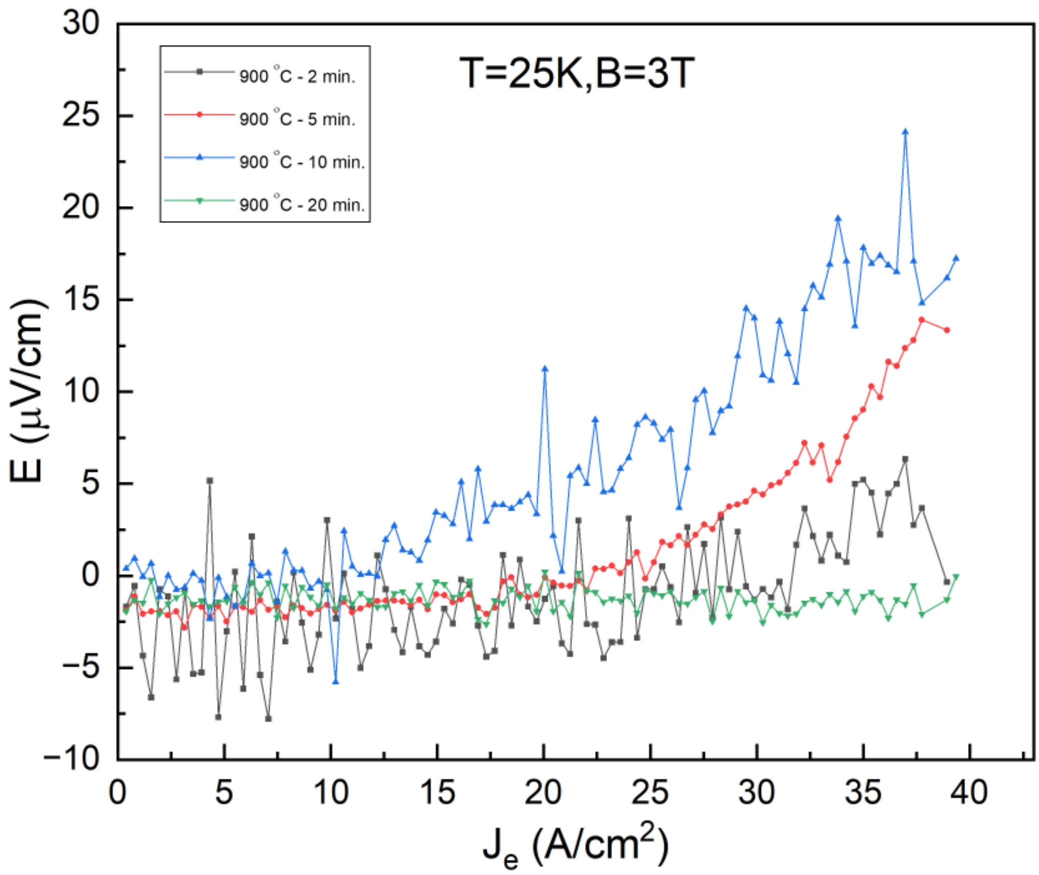

Figure 8.11. Je vs. E curve for the sintered samples at 900 °C for durations of 2, 5, 10, and 20 minutes at an external magnetic field of 3 Tesla and a critical temperature of 25 K.

8.3 Scanning Electron Microscope (SEM) Analysis

The surface analyzes of the samples were performed using JEOL brand scanning electron microscope, model 6390- LV, in Bolu Abant İzzet Baysal University Faculty of Arts and Sciences. Detailed SEM images for different samples in different scales from picture 8.2 to 8.9. Picture 8.2 contains images of cross-sectional surfaces of unreacted and reacted samples. These images were taken after the surfaces of the samples were sanded (Picture 8.1). As you can see, the wires have a perfectly regular circular structure.

Pictures 8.2 through 8.9 show SEM photographs of the samples heat treated for 2 minutes at various temperatures and 900 °C for various times, taken at 100, 1000, and 3000 magnifications. In general, the samples contain voids, pores, and cracks. However, as can be seen from the resistivity versus temperature curves and the I-V results, it is clear that these structures do not prevent the formation of superconductivity and current carrying of the samples. However, as we know from the literature and our experience, the denser the core of a sample, the higher its current carrying capacity. When we examined the picture of each sample showing the transition from the core region to the iron sheath, no iron oxide-like structures were found. Therefore, we can say that induction heating, which we performed in an argon atmosphere, works very well at this point.

Picture 8.1. Sanded sample.

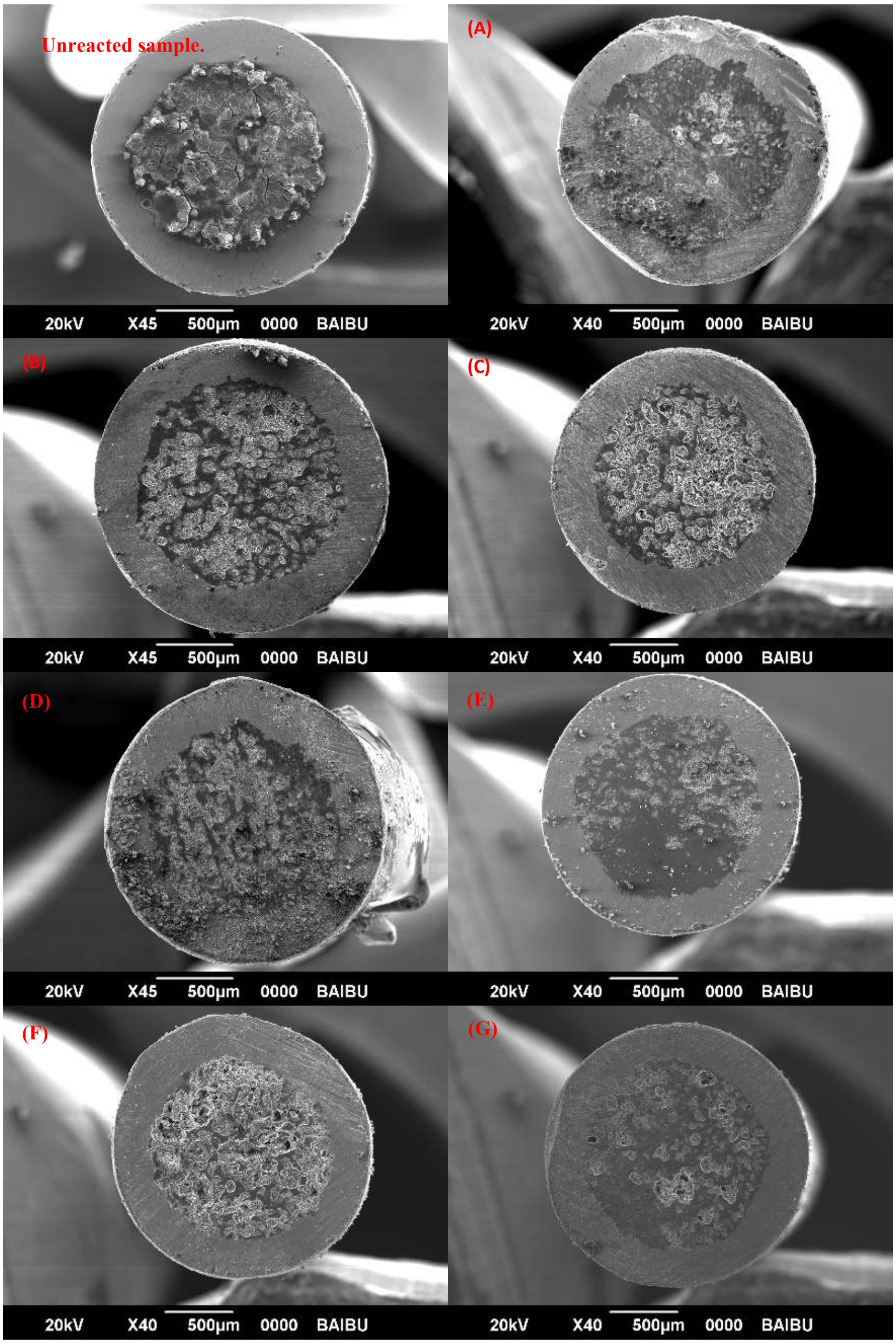

Picture 8.2. Cross-sectional SEM pictures of the samples, unreacted and A, B, C, D, E, F, G.

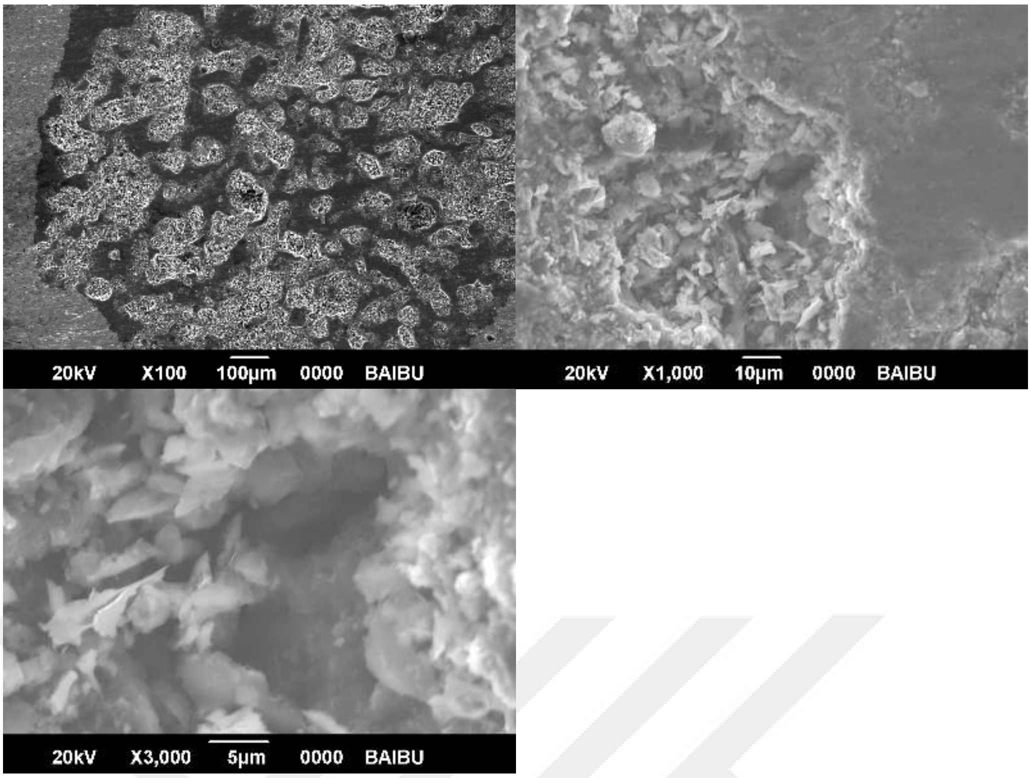

Picture 8.3. Sample A, 800 °C 2 minutes.

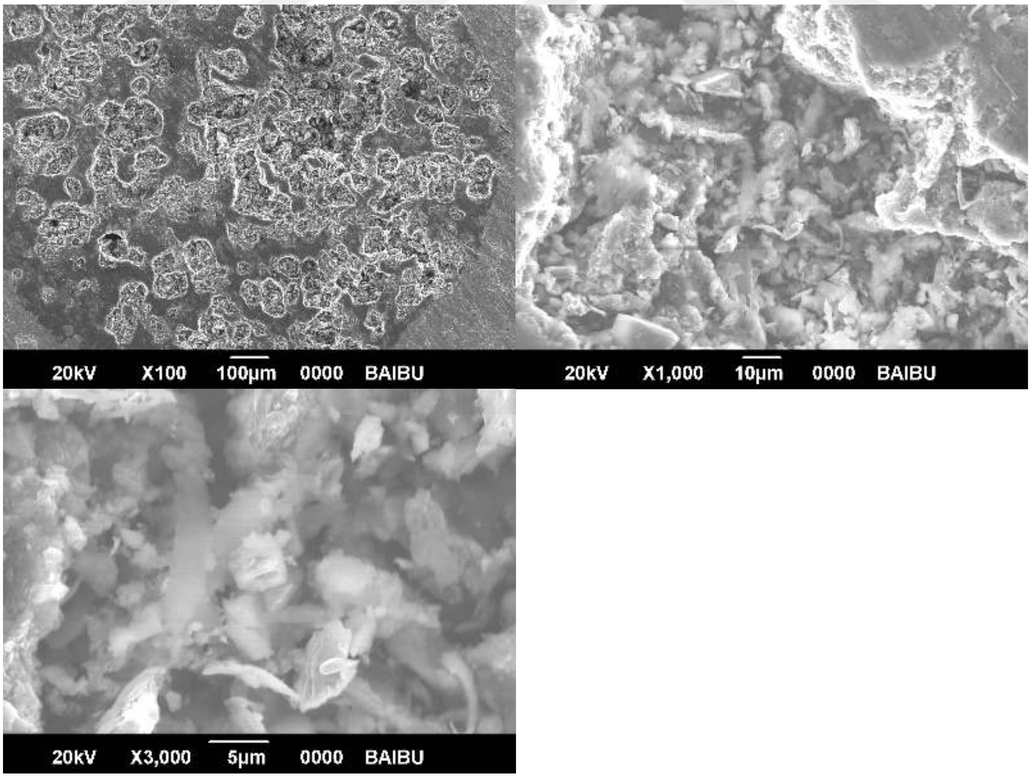

Picture 8.4. Sample B, 850 °C 2 minutes.

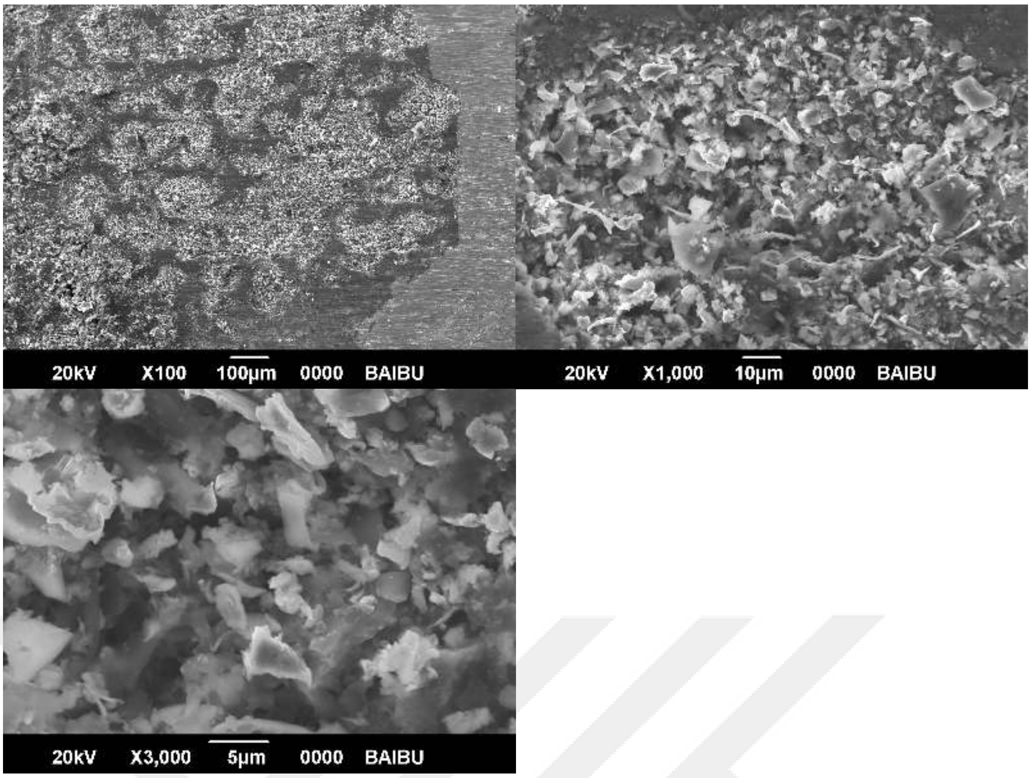

Picture 8.5. Sample C, 900 °C 2 minutes.

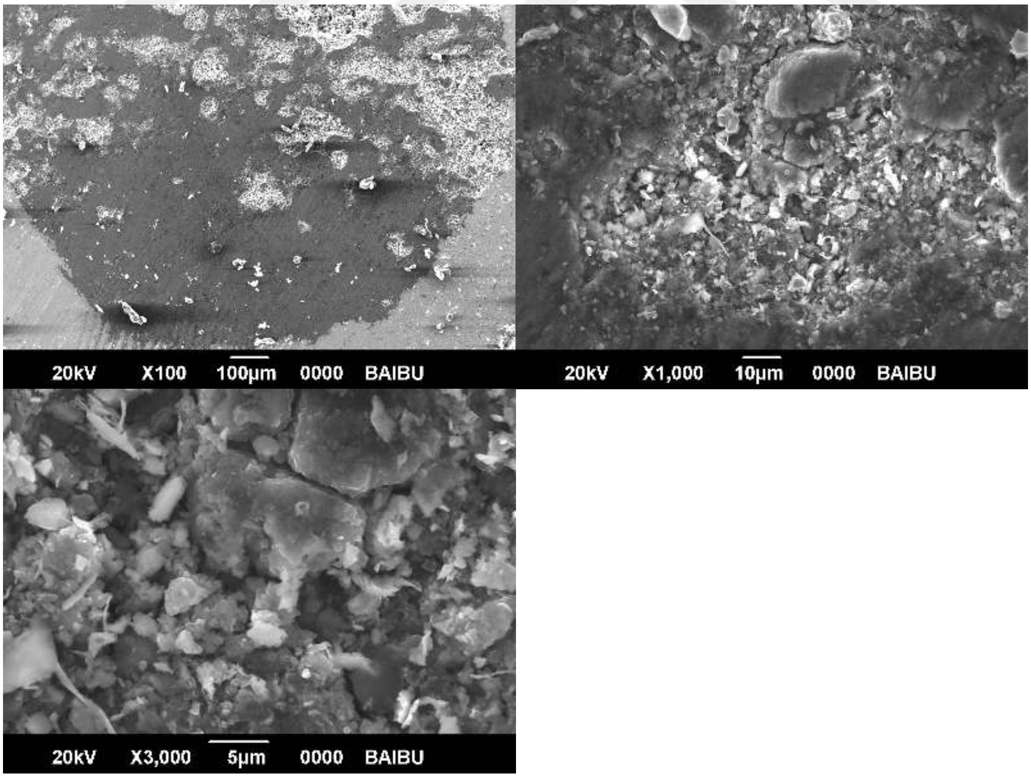

Picture 8.6. Sample D, 900 °C 5 minutes.

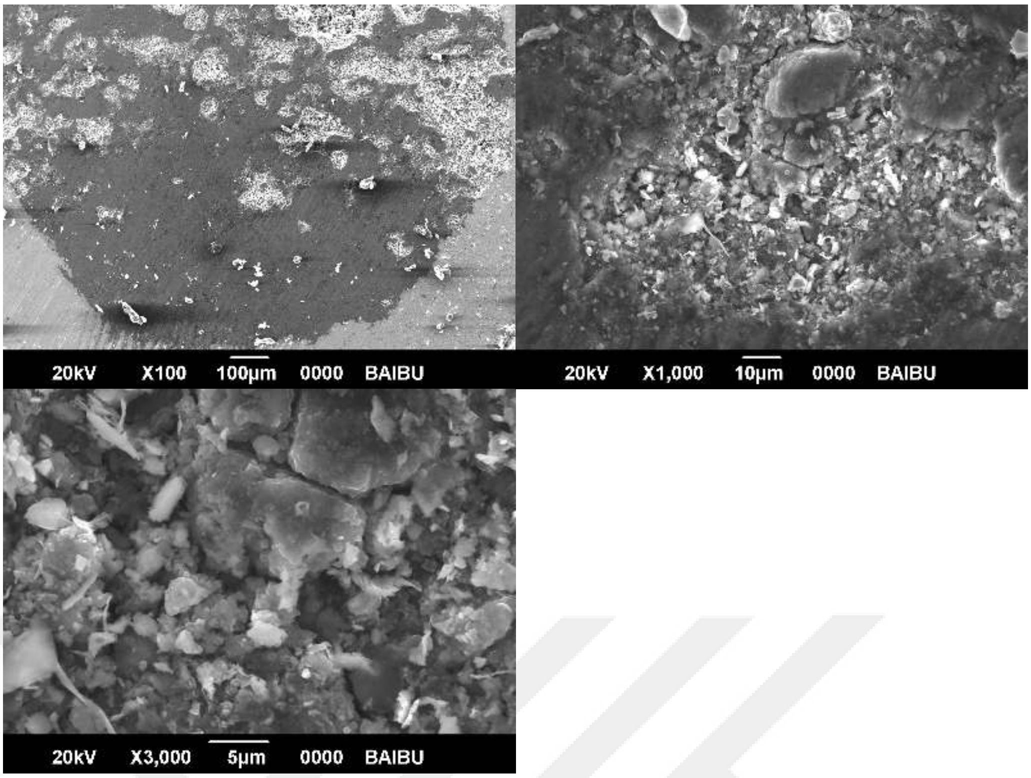

Picture 8.7. Sample E, 900 °C 10 minutes.

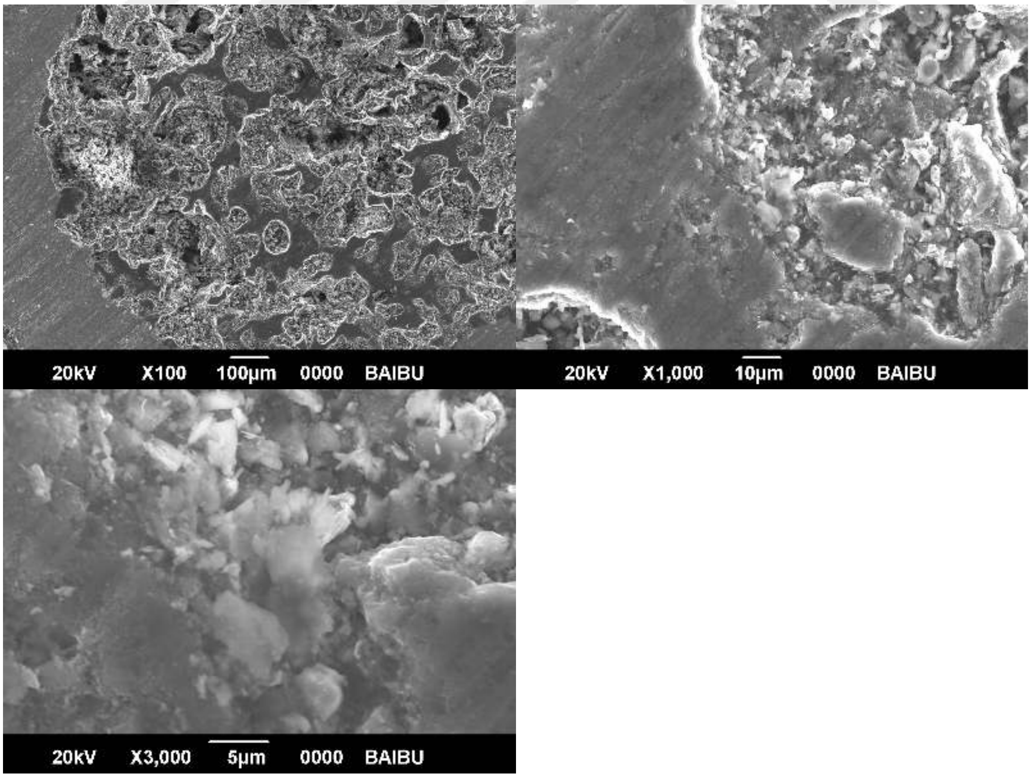

Picture 8.8. Sample F, 900 °C 20 minutes.

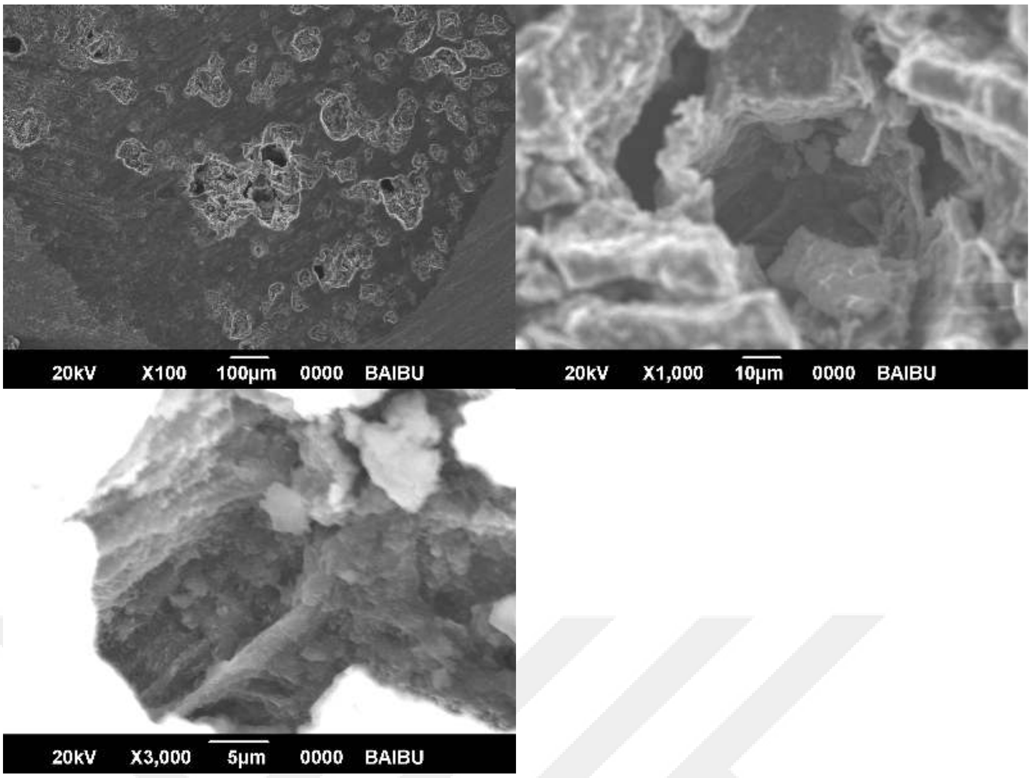

Picture 8.9. Sample G, 950 °C 2 minutes.

8.4 XRD Analysis

X-ray analyzes were performed using the Rigaku MultiFlex+ device in the Bolu Abant İzzet Baysal College Faculty of Arts and Sciences. We intended to remove the iron jacket on the outer surface of the samples for analysis, but the very small diameter of the sample, its fragile structure and we did not want to lose the sample, which prevented us from doing so. For this reason, we prepared the samples for analysis by abrading the samples longitudinally with sandpaper to half the sample diameter so that both the iron and the core portion were visible. We performed the analysis at a rate of 3 degrees/minute in the range of 5 to 90 degrees.

Figures 8.12 and 8.13 show the results of X-ray analysis of the samples heat treated at different temperatures for 2 minutes and at 900 °C for different times, respectively. In both figures, the peaks of iron, iron oxide, magnesium oxide, and magnesium diboride are labeled. There are some unlabeled peaks in the figures that are from the substrate on which the sample lies.

In Figure 8.12, the intensity of the iron oxide peaks decreases with increasing temperature. It can also be observed that the main MgB_2 peak, which is at about 42 degrees, increases from 800 to 950 °C, while the iron oxide phase decreases up to 900 °C, but increases at 950 °C. The presence of magnesium oxide peaks is clearly visible at any temperature. From these results, we conclude that, in general, 2-minute induction heating is sufficient to achieve a superconducting phase transition in the MgB_2/Fe sample.

Figure 8.13 shows the X-ray analyzes of samples heat treated at 900 degrees for various times. If we look at the iron oxide peaks, 2 and 20 minutes have similar intensities, while 5 and 10 minutes have similar intensities. When we compare the MgB2 main phase, the peak intensity decreases with increasing duration up to 20 minutes and increases again at 20 minutes. The results can be somewhat misleading because the sample sizes are too small for analysis. Again, magnesium oxide peaks are seen, but peak intensities decrease with increasing duration.

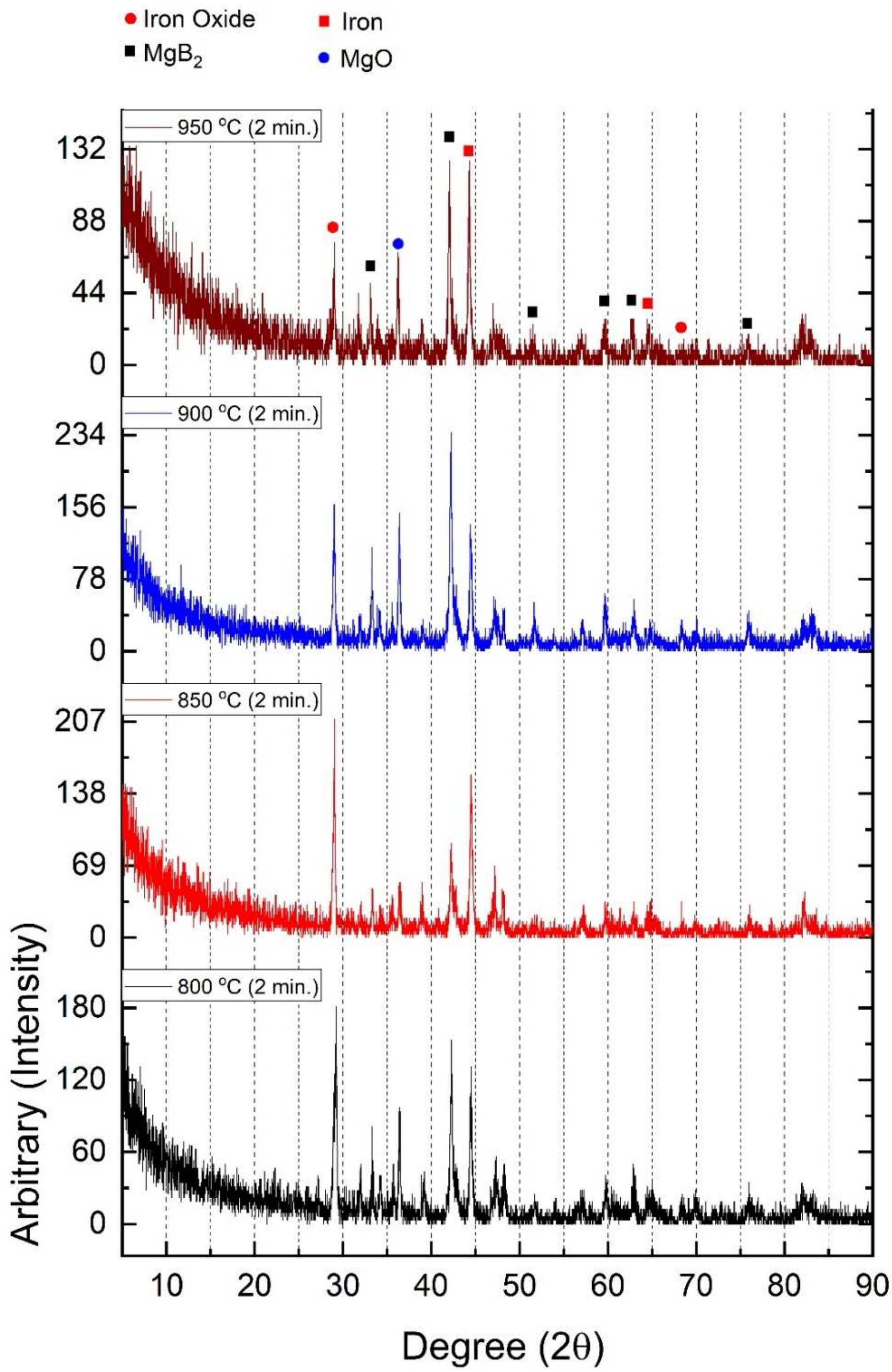

Figure 8.12. XRD patterns of all samples heat treated at 800, 850, 900, and 950 °C in 2 minutes.

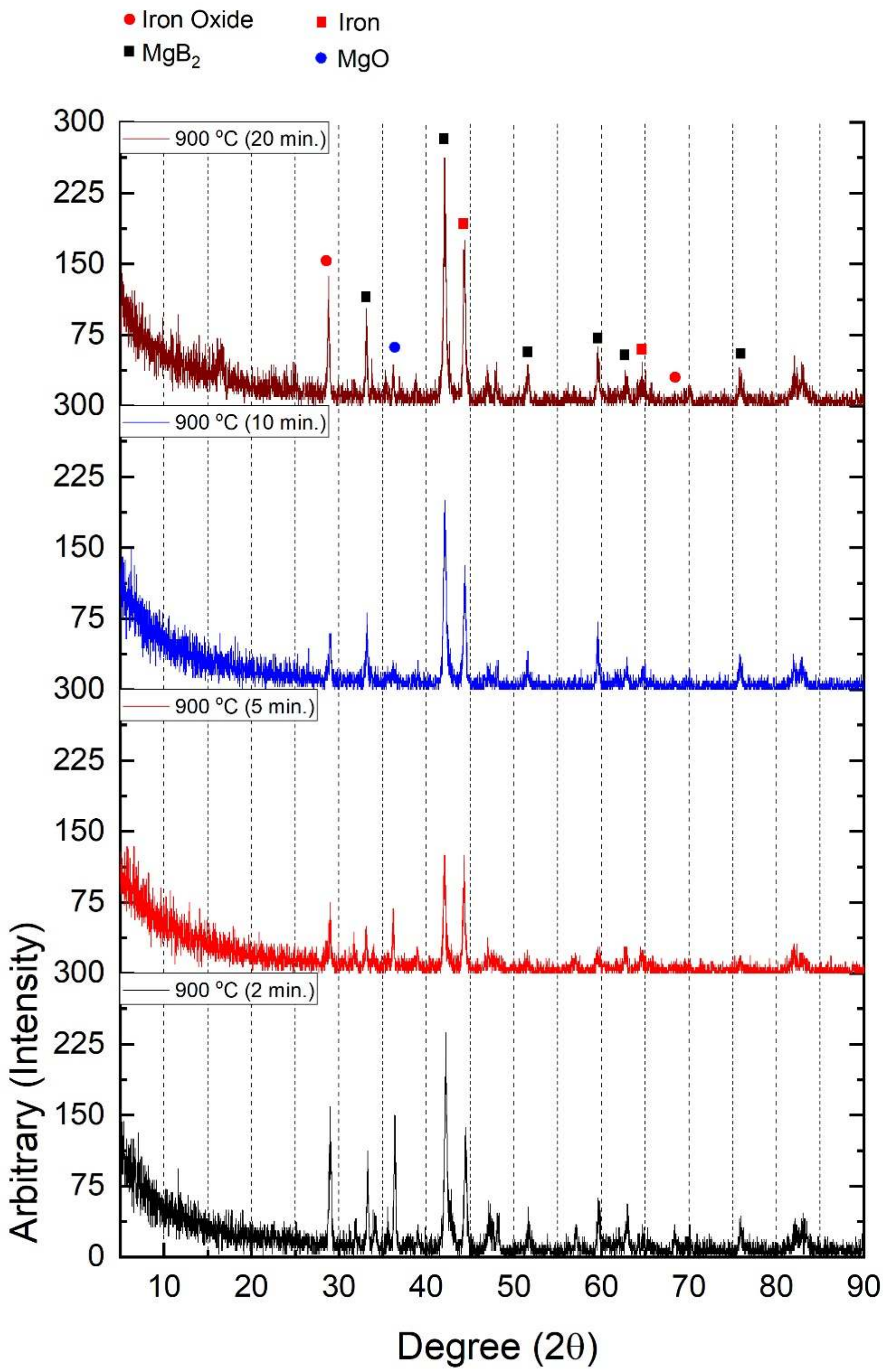

Figure 8.13. XRD patterns of the samples heat treated at 900 °C for 2, 5, 10 and 20 minutes.

9. CONCLUSION

At the beginning of this study, our aim was to develop an alternative heat treatment method to the time and energy we lose while doing heat treatment with conventional furnaces. Based on this idea, we developed the induction heater in a laboratory environment with our own means. We calibrated the induction heater we developed with the Fluke Ti300+ thermal camera from our university. Again, with our own means, we had a quartz tube made in which we can heat the wire in the gas flow atmosphere. We connected the pipe extending from the argon tube to one end of the quartz tube. We placed our wire samples, both ends of which were closed with a mechanical press, from the other end of the quartz tube and performed the heat treatment inside the induction coil with an argon flow athmosphere. We investigated the electrical/superconductivity effects of heat treatment in terms of both temperature and time. We made resistance-temperature and magnetoresistance-temperature measurements in our cryostat system with a 7 T magnetic field by cutting samples of approximately 2-2.5 cm in length from the middle parts of our wires, whose heat treatment was completed. In addition, we performed both XRD and SEM analyzes by sanding these samples up to half the diameter with paper sandpaper. We explained our results in detail in the results and discussion section. In short, with this study, we carried out the heat treatment of our 1.8 mm diameter iron sheathed MgB_2 wire in a short time of 2 minutes with an energy of approximately 90W and compared the properties of our samples with the same wire heat-treated in a tube furnace at the same temperature. The heat treatment in the tube furnace takes a total of 6 hours, including the heating and cooling steps, and the energy consumed during this time is approximately 7.2 kW (the tube furnace consumes 1.2 kW of energy per hour). Even in this respect alone, significant time and energy savings have been achieved. As a result of the tests and analyzes, it was determined that the samples with the best transition temperature were the C and D samples, but it was not known which sample was the best current-carrying sample. As we stated in the Results and Discussion section, the measurements should be performed in a liquid helium environment to determine the sample with the best current-carrying capability.

As a result, with this study, we have developed the induction heater, which is an alternative heat treatment method in terms of both time and energy use to the heat treatments with conventional furnaces. In this study, we observed that the induction heater is a practical heat treatment tool that is environmentally friendly and activated very quickly. In our future work, we plan to give a new direction to our work by developing an adjustable frequency induction heater.

10. REFERENCES

Vancouver citation style was used in this thesis.

1. Matera D, Bonura M, Barth C, Fete A, Cerny R, Giannini E, et al. Rapid synthesis of MgB2 by inductive heating. IEEE Transactions on Applied Superconductivity. 2018;28(4):1–5.

2. Jie L, Jianwei M, Xiangcheng Z. Design of host computer system for induction heating power supply based on LabVIEW. In: Proceedings of 2020 IEEE 2nd International Conference on Civil Aviation Safety and Information Technology, ICCASIT 2020. Institute of Electrical and Electronics Engineers Inc.; 2020. p. 639–42.

3. Nagamatsu J, Nakagawa N, Muranaka T, Zenitani Y, Akimitsu J. Superconductivity at 39 K in magnesium diboride. Nature [Internet]. 2001 Mar;410(6824):63–4. Available from: https://www.nature.com/articles/35065039

4. Runde M, Stenvall A, Magnusson N, Grasso G, Mikkonen R. MgB2 coils for a DC superconducting induction heater. J Phys Conf Ser. 2008 Feb 1;97(1).

5. Zhang D, Dai ST, Wang ZK, Zhang JY, Song NH, Li XH, et al. Research on stability of MgB2 superconducting magnet for MRI. IEEE Transactions on Applied Superconductivity. 2011 Jun;21(3 PART 2):2100–3.

6. Ling J, Voccio J, Kim Y, Hahn S, Bascunan J, Park DK, et al. Monofilament MgB2 wire for a whole-body MRI magnet: Superconducting joints and test coils. IEEE Transactions on Applied Superconductivity. 2013;23(3).

7. Patel D, Matsumoto A, Kumakura H, Maeda M, Kim SH, Liang H, et al. Superconducting joints using multifilament MgB2 wires for MRI application. Scr Mater. 2021 Nov 1;204.

8. Ballarino A, Bruzek CE, Dittmar N, Giannelli S, Goldacker W, Grasso G, et al. The BEST PATHS Project on MgB2 Superconducting Cables for Very High Power Transmission. IEEE Transactions on Applied Superconductivity. 2016 Apr 1;26(3).

9. Kostyuk V V., Antyukhov I V., Blagov E V., Vysotsky VS, Katorgin BI, Nosov AA, et al. Experimental hybrid power transmission line with liquid hydrogen and MgB 2-based superconducting cable. Technical Physics Letters. 2012 Mar;38(3):279–82.

10. Magnusson N, Eliassen JC, Abrahamsen AB, Helleso SM, Runde M, Nysveen A, et al. Fabrication of a Scaled MgB2 Racetrack Demonstrator Pole for a 10-MW Direct-Drive Wind Turbine Generator. IEEE Transactions on Applied Superconductivity. 2018 Jun 1;28(4).

11. Kalsi SS. Superconducting Wind Turbine Generator Employing MgB2 Windings Both on Rotor and Stator. IEEE Transactions on Applied Superconductivity. 2014 Feb 1;24(1).

12. Magnusson N, Hellesø SM, Mikkonen R, Abrahamsen AB, Runde M, Berg G, et al. Testing of an MgB2 coil for a wind turbine generator pole. Physica C: Superconductivity and its Applications. 2021 Aug 15;587.

13. Morandi A, Fiorillo A, Pullano S, Ribani PL. Development of a Small Cryogen-Free MgB2 Test Coil for SMES Application. IEEE Transactions on Applied Superconductivity. 2017 Jun 1;27(4).

14. Kwon J, Rochester J, Wan F, Rindfleisch MA, Tomsic MJ, Sumption MD, et al. Critical Current Densities and n-Values of MgB_2 Conductors for SMES, MRI, and Low AC Loss Applications. IEEE Transactions on Applied Superconductivity. 2023 Aug 1;

15. Morandi A, Fabbri M, Ribani PL, Lo Franco F, Mandrioli R, Melaccio U, et al. Calculation of AC Losses in a 500 kJ/200 kW Multifilamentary MgB2 SMES Coil. Energies (Basel). 2023 Feb 1;16(4).

16. Akdoğan M, Yetiş H, Gajda D, Karaboğa F, Rogacki K, Morawski A, et al. Use of amorphous boron and amorphous nano boron powder mixture in fabrication of long in-situ MgB2/Fe wires. J Alloys Compd. 2017;702:399–403.

17. Matsumoto A, Hatakeyama H, Kitaguchi H, Togano K, Kumakura H. The superconducting properties of MgB2/(stainless steel) tapes fabricated by the PIT process. In: IEEE Transactions on Applied Superconductivity. 2003. p. 3225–8.

18. Balamurugan S, Nakamura T, Osamura K, Muta I, Hoshino T. Structural and superconducting properties of PIT processed sintered MgB2/Fe wires. In: Physica C: Superconductivity and its Applications. 2004. p. 1184–8.

19. Kodama M, Tanaka K, Okamoto K, Yamamoto A, Shimoyama JI. Effect of the premixing of MgB2 powder on microstructures and electromagnetic properties in PIT-processed MgB2 wires. Mater Res Express. 2019 Feb 1;6(2).

20. Karaboğa F, Yetiş H, Akdoğan M, Belenli İ. Monofilamentary In Situ Fe/MgB2 Superconducting Wires Fabricated by Pellet-in-Tube Method. J Supercond Nov Magn. 2018 May 1;31(5):1359–67.

21. Suo HL, Ma L, Jiang JM, Li YM, Zhang ZL, Liu M, et al. High critical current densities in SiC doped in-situ MgB2 wires prepared by continuous tube forming and filling technique. In: IEEE Transactions on Applied Superconductivity. 2007. p. 2822–5.

22. Ma L, Suo HL, Zhang ZL, Gao TY, Liu M, Zhao Y, et al. Preparation of SiC doped In-Situ MgB2 mono- and 7-filamentary wires by continuous tube forming and filling technique. J Phys Conf Ser. 2008 Feb 1;97(1).

23. Balachandran U. Advances in cryogenic engineering : transactions of the International Cryogenic Materials Conference (ICMC), Anchorage, Alaska 22-26 September 2003. American Institute of Physics; 2004.

24. Egilmez M, Ozyuzer L, Tanoglu M, Okur S, Kamer O, Oner Y. Electrical and mechanical properties of superconducting MgB2/Mg metal matrix composites. Supercond Sci Technol. 2006;19(4):359–64.

25. Ploetz S, Nowak R, Lohmueller A, Sobczak N, Singer RF. Wettability of Low Weight Borides by Commercial Aluminum Alloys − A Basis for Metal Matrix Composite Fabrication. Adv Eng Mater. 2016 Nov 1;18(11):1884–8.

26. Kováč P, Kopera L, Kováč J, Hain M, Melišek T, Kulich M, et al. Rutherford cable made of internal magnesium diffusion MgB2 wires sheathed with Al-Al2O3 particulate metal matrix composite. Supercond Sci Technol. 2018 Jan 1;31(1).

27. Kortus J, Mazin II, Belashchenko KD, Antropov VP, Boyer LL. Superconductivity of metallic Boron in MgB2. Phys Rev Lett. 2001;86(20):4656–9.

28. Choi HJ, Roundy D, Sun H, Cohen ML, Louie SG. First-principles calculation of the superconducting transition in MgB2 within the anisotropic Eliashberg formalism. Phys Rev B Condens Matter Mater Phys. 2002;66(2):205131–4.

29. Koshelev AE, Golubov AA. Why Magnesium Diboride Is Not Described by Anisotropic Ginzburg-Landau Theory. Phys Rev Lett. 2004;92(10):12–5.

30. Xu M, Kitazawa H, Takano Y, Ye J, Nishida K, Abe H, et al. Anisotropy of superconductivity from MgB2 single crystals. Appl Phys Lett. 2001;79(17):2779–81.

31. Lima OF De, Cardoso CA. 3 Upper Critical Field Anisotropy. 2003;33(4):709–12.

32. Angst M, Puzniak R, Wisniewski A, Jun J, Kazakov SM, Karpinski J, et al. Temperature and field dependence of the anisotropy of MgB2. Phys Rev Lett. 2002;88(16):1670041–4.

33. Mikheenko P, Martínez E, Bevan A, Abell JS, MacManus-Driscoll JL. Grain boundaries and pinning in bulk MgB2. Supercond Sci Technol. 2007;20(9).

34. Martínez E, Mikheenko P, Martínez-López M, Millán A, Bevan A, Abell JS. Flux pinning force in bulk Mg B2 with variable grain size. Phys Rev B Condens Matter Mater Phys. 2007;75(13):1–8.

35. Naito T, Endo Y, Fujishiro H. Optimization of vortex pinning at grain boundaries on ex-situ MgB2 bulks synthesized by spark plasma sintering. Supercond Sci Technol. 2017;30(9).

36. Jiang CH, Nakane T, Hatakeyama H, Kumakura H. Enhanced Jc property in nano-SiC doped thin MgB2/Fe wires by a modified in situ PIT process. Physica C: Superconductivity and its Applications. 2005;422(3–4):127–31.

37. Pan A V., Zhou S, Liu H, Dou S. Properties of superconducting MgB2 wires: In situ versus ex situ reaction technique. Supercond Sci Technol. 2003;16(5):639–44.

38. Chen SK, Majoros M, MacManus-Driscoll JL, Glowacki BA. In situ and ex situ Cu doping of MgB2. Physica C: Superconductivity and its Applications. 2005;418(3–4):99–106.

39. Edison S, Via S, Milano UB. HIGH DENSITY MgB 2 OBTAINED BY REACTIVE LIQUID Mg INFILTRATION GIOVANNI GIUNCHI. Physics (College Park Md). :2–9.

40. Li GZ, Yang Y, Susner MA, Sumption MD, Collings EW. Critical current densities and n-values of MgB 2 strands over a wide range of temperatures and fields. Supercond Sci Technol. 2012;25(2).

41. Shimada Y, Hata S, Ikeda K ichi, Nakashima H, Matsumoto A, Togano K, et al. Infiltration behavior of molten Mg and its influence on microstructural evolution in

SiC-doped MgB2 wires prepared by internal Mg diffusion process. J Alloys Compd. 2018;740:305–11.

42. Collings EW, Lee E, Sumption MD, Tomsic M, Wang XL, Soltanian S, et al. Continuous- and batch-processed MgB2/Fe strands - Transport and magnetic properties. Physica C: Superconductivity and its Applications. 2003;386:555–9.

43. Gajda D, Morawski A, Zaleski AJ, Cetner T, Häßler W, Nenkov K, et al. Significant enhancement of the critical current of MgB2 wires through a reduction of the diameter using HIP method. Scr Mater. 2018;143:77–80.

44. Jie H, Qiu W, Billah M, Mustapic M, Patel D, Ma Z, et al. Superior transport Jc obtained in in-situ MgB2 wires by tailoring the starting materials and using a combined cold high pressure densification and hot isostatic pressure treatment. Scr Mater. 2017;129:79–83.

45. Hossain MSA, Motaman A, Barua S, Patel D, Mustapic M, Kim JH, et al. The roles of CHPD: Superior critical current density and n-value obtained in binary in situ MgB2 cables. Supercond Sci Technol. 2014;27(9).

46. Akdoɫan M, Yetiş H, Gajda D, Karaboɫa F, Ülgen AT, Demirtürk E, et al. Effect of the initial filling density on the critical current of in-situ Fe/MgB2 wires. J Alloys Compd. 2015;649:1007–10.

47. Ngoc HP, Fujita H, Ozaki K, Uchida N. Phase angle control of high-frequency resonant currents in a multiple inverter system for zone-control induction heating. IEEE Trans Power Electron. 2011;26(11):3357–66.

48. Fujita A, Sadakata H, Hirota I, Omori H, Nakaoka M. Latest developments of high-frequency series load resonant inverter type built-in cooktops for induction heated all metallic appliances. 2009 IEEE 6th International Power Electronics and Motion Control Conference, IPEMC '09. 2009;3:2537–44.

49. Dawson FP, Jain P. A Comparison of Load Commutated Inverter Systems for Induction Heating and Melting Applications. IEEE Trans Power Electron. 1991;6(3):430–41.

50. Park JS, Taniguchi S, Park YJ. Maximum Joule heat by tubular susceptor with critical thickness on induction heating. J Phys D Appl Phys. 2009;42(4).

51. Boadi AK, Shimoji H, Todaka T, Enokizono M. Designing of suitable construction of high-frequency induction coil by using finite element method. INTERMAG ASIA 2005: Digests of the IEEE International Magnetics Conference. 2005;41(10):1077–8.

52. Subhi El-bayyari Z. Health Sciences Course Syllabus Course Title: General Physics For Health Sciences Course Level : 1 Course Code : 211109 Course Prerequisite(s): N/A. Physics Program General Physics Course. 211AD;(0211109).

53. Stauffer PR, Cetas TC, Jones RC. Magnetic Induction Heating of Ferromagnetic Implants for Inducing Localized Hyperthermia in Deep-Seated Tumors. IEEE Trans Biomed Eng. 1984;BME-31(2):235–51.

54. Tai CC, Chen CC, Kuo CC, Lin FW, Chang CJ, Chen YH, et al. Deep-magnetic-field generator using flexible laminated copper for thermotherapy applications. IEEE Trans Magn. 2014;50(11):1–4.

55. Choi J, Kim SK, Kim K, Park M, Yu IK, Kim S, et al. Design and performance evaluation of a multi-purpose HTS DC induction heating machine for industrial applications. IEEE Transactions on Applied Superconductivity. 2015;25(3):1–5.

56. Egalon J, Caux S, Maussion P, Souley M, Pateau O. Multiphase system for metal disc induction heating: Modeling and RMS current control. IEEE Trans Ind Appl. 2012;48(5):1692–9.

57. Vijendra B, Sharma A. Induction heated tool assisted friction-stir welding (i-FSW): A novel hybrid process for joining of thermoplastics. J Manuf Process. 2015;20:234–44.

58. Mungikar H, Jape S. Trends in energy conservation technology: Temperature control of induction cooking application using class e resonant inverter. International Conference on Energy Systems and Applications, ICESA 2015. 2016;(Icesa):214–9.

59. Vishnuram P, Ramasamy S, Suresh P, Sureshkumar A. A simple digital control for mitigating voltage stress on single switch resonant inverter for induction cooking applications. International Journal of Electronics Letters. 2020;8(2):162–9.